People's Democratic Republic of Algeria
Ministry of Higher Education and Scientific Research
Tissemsilt University

Faculty of Sciences and Technology
Department of Sciences and Technology

Dissertation submitted in fulfillment of the requirements for the degree of academic Master in

Stream: **Mechanical Engineering**

Specialty: **Energy Installations and Turbomachines**

Realized by: **BENTAMRA Mohamed Tayeb**

Theme

Numerical study of a turbulent flow in a ''mixing T-junction''

2022

Board of Examiners:

Dr. BENLEKKAM M.E.	President	Tissemsilt University
Dr. KAHIL Y.	Supervisor	Tissemsilt University
Dr. BAGHDAD M.	Examiner	Tissemsilt University

2021-2022

République Algérienne Démocratique et Populaire

Ministère de l'Enseignement Supérieur

et de la Recherche Scientifique

Université de Tissemsilt

Faculté des Sciences et de la Technologie

Département des Sciences et de la Technologie

Mémoire de fin d'études pour l'obtention du diplôme de Master académique en
Filière: **Génie Mécanique**

Spécialité: **Installations Energétique et Turbomachines**

Réalisé par: **BENTAMRA Mohamed Tayeb**

Thème

Etude numérique d'un écoulement turbulent dans un ''T de mélange''

2022

Devant le Jury:

Dr. BENLEKKAM M.E.	Président	Université de Tissemsilt
Dr. KAHIL Y.	Encadrant	Université de Tissemsilt
Dr. BAGHDAD M.	Examinateur	Université de Tissemsilt

Année universitaire : 2021-2022

Dedication

“Everything I am or ever will be, I owe it to my father and my mother

My success is because of her prayer for me

To you mother.

“To my biggest supporter

To you father “

To all my family

Acknowledgments

All the gratitude and thanks to Allah our creator who has given us the strength to carry out and complete this work.

First of all, I would like to thank the members of the jury, the president ***Dr. BAGHDAD M.*** *and* ***Dr. BENLEKKAM M.E****. to agree to examine this modest memory.*

I would like to thank my promoter very warmly ***Dr. KAHIL Y.*** *for having proposed this subject to me, for its precious advice for his open-mindedness and availability.*

Many thanks to all the professors of the department of Sciences and Technology for their contributions to my education and training, and my knowledge.

TABLE OF CONTENTS

List of figures

List of tables

Nomenclature

D	Diameter [m]
L	Length [m]
λ/Dm	Wavelength ratio
a/Dm	Amplitude ratio
M	Mass [Kg]
ρ	Fluid density [$Kg.m^{-3}$]
U	Mean fluid velocity [$m.s^{-1}$]
P	Pressure [$Kg.m^{-1}.s^{-2}$]
$\vec{A}$	Surface area vector
C_{μ}	Constants of the K-ε model
μ	Dynamic viscosity of the fluid [$P_a s^{-1}$]
u′	Fluctuating component
N	Grid number
Re	Reynolds number
$\overline{u}$	Time-averaged velocity
s_{ij}	Train-rate tensor
v_T	Turbulent eddy viscosity
k	Turbulence kinetic energy
v	Molecular viscosity
C_{w1}	ω Production
Ω_{ij}	Rotation tensor
$C_{\varepsilon 1}, C_{\varepsilon 2}, \delta_k, \delta_\varepsilon$	Coefficients of k-ε modeling
$\overline{u_i' u_j'}$	Components of Reynolds tensor.
$\alpha, \beta_0^*, \sigma, \sigma^* \beta_0, \sigma_{do}$	Coefficients of k-ω modeling
P_k	Production limiter
F_1	Blending function
F_2	Second blending function
$\beta^*, \alpha_1, \beta_1, \sigma_{k1}, \sigma_{\omega 1}, \alpha_2, \sigma_{k2}, \sigma_{\omega 2}$	Coefficients of k-ω-SST model
$\vec{v}$	Velocity vector $\left(\vec{v} = v_x \vec{\imath} + v_y \vec{\jmath}\right)$
C_p	Specific heat
λ	Thermal conductivity
G	Gap distance
$\bar{P}$	Mean pressure

GENERAL INTRODUCTION

Introduction:

The turbulent flow is irregular, and it is difficult to predict because it is complex and has a movement in all directions, as we cannot accurately calculate the movement of turbulence and the properties of the fluid only approximate or obtain results that give us a general idea of the flow.**[1]**

Obviously, we witness a lot of these phenomena in our daily life, for example, the flow of smoke from fire, smoke from aircraft engines, the flow of water in rivers, cloud flow and flow in water pipes especially where two liquids are mixed, so we find this interest shown by technicians and engineers in the study of turbulent flow, and therefore it is important to know the nature and study of this flow

The costs of the experimental method are often expensive in order to search for a solution to a problem or to develop a product or production line, which leads to a waste of money, time and effort that may be destroyed, these expensive experiments represented an obstacle to rapid progress and solving problems, especially in terms of industrial development and saving energy and time, as the ideas applied to industry were basic ideas in principle, so it was necessary to change the situation in scientific research so that we can develop these Ideas and principles without big costs and great waste of energy and time.

We noticed the extent of development that happened in computers for simulation, especially in the last decade, where these devices realties a performing complex simulations in a short period, in addition, there was an evolution in the method of modeling the turbulent flow.

Starting with the first Course in Turbulence, Tennekes & Lumley (1972) Cambridge, (The Taylor microscale, which is sometimes called the turbulence length scale, is a length scale used to characterize a turbulent fluid flow) **[2]**, to the model that best fits our study k-ω - SST Model (2006).

CFD codes are now used to deal with complex flow simulations, and produce more accurate results in a short time. This made CFD a reliable and chosen method in solving problems related to fluid flow , heat transfer, mass transfer, and chemical reactions. [3]

Among the most important problems studied in computational fluid mechanics, is the flow in a T-junction channel, so we will study in a T-junction flow with two inlets and an outlet for flow and smooth walls, in dynamic simulation, the temperature of fluid is constant, and in dynamic and thermal simulation, the fluid temperature in one inlet is different from the other. [4]

The manuscript is divided into five chapters. We start with bibliographic analysis; Chapter 2 deals with turbulence modeling. Chapter 3 concerns the numerical resolution of all free software used for this work. Chapter 4 presents the case study, followed by the results and discussion. Finally, we conclude with a general conclusion that brings together the main points of our research.

CHAPTER 1: BIBLIOGRAPHIC ANALYSIS

Introduction

The literature that covers the field of flow study T-junction, which is among the most important problems and studies in fluid mechanics, is shown below.

Westin, J. (2007). [5]

The Älvkarleby laboratory of Vattenfall Research and Development in Sweden carried out in vitro experiments where two liquids were mixed using the T-junction connection. The results of the experiment became available in November 2008 from the Älvkarleby laboratory. These data are the basis for verifying the quality of CFD simulation results.

Kuczaj, A. K. and Komen, E. M. J. (2010) [6]

The effect of heat stress at the T junction was studied using large simulation models and the simulation results were compared with experimental data. It was concluded in this research that in order to obtain the computational results of the simulation close to the experimental results, it is necessary to resolve the Taylor micro-scale length ($\Delta \sim \frac{\lambda}{3}$) or should be of the order of Taylor micro-scale obtained from the RANS simulations ($\Delta \sim R_{\lambda}$), a fine mesh should be used near the center in order to obtain adequate results for the flow characteristics at the mixing center at the T junction.

Walker, C., Manera, A., Niceno, B., Simiano, M. and Prasser, H. M. (2010) [7]

Presented a steady-state RANS-simulations of the mixing T-junction. Two streams of water with a different concentration of dissolved ions were mixed. Calculations were performed with ANSYS-CFX using the k–ε, SST and BLS Reynolds stresses models.

Aulery, F., Toutant, A., Monod, R., Brillant, G. and Bataille, F. (2012) [8]

The capacity and temperature fluctuations with high differences in a Phenix pool type reactor were studied using RANS or LES rates, and it was found that the crack areas in the pipes correspond to the high thermal fluctuation areas at the T junction. A high flow of heat between the walls and the liquid was observed, and a significant transfer of heat was observed at the interfluid (wall/liquid).

Ayhan, H. and Sökmen, C. N. (2013) [9]

Thermal fatigue was studied at the T-junction with a calibration in the sub-inlet diameter, which depended on three ratios of the sub-diameter to the main diameter, which are 0.571, 0.714 and 0.857, and with respect to the sub-inlet temperature 36 degrees Celsius and the temperature of the main shaft 19 degrees Celsius. Test cases are simulated by Computational Fluid Dynamics (CFD) code using Large Eddy Simulation (LES) turbulence model. As branch duct hydraulic diameter increases (also velocity or momentum ratio decreases), magnitude of thermal load decreases, on the other hand, intensity of thermal load does not change, “A” decreases but “B” increases. The magnitude of thermal load depends on temperature difference of fluids.

Temperature fluctuations become considerably important if their magnitude is high. The results provide information about the lifetime of mixing tees exposed to thermal load. Analysis of the temperature fluctuations shows that the frequency range of 2-5 Hz contains most of the energy, in accordance with the results of the previous studies, therefore, may cause fatigue.

Howard, R. J. A. and Serre, E. (2015) [10]

The temperature fluctuations and thermal fatigue on the walls of industrial pipes in the T-junction have been studied using the large Eddy simulation model LES and the average Reynolds number is greater than 39080, and this is due to two different conditions of the thermal limits of the walls, in the first condition there is heat transfer between the liquid and the walls, while the second is isolated. In this research, it was concluded that the velocity and temperature field is not affected by the heat transfer with the walls, but the temperature fluctuations are not the same, which indicates that the thermal fluctuations on the walls cannot be predicted by knowing the thermal fluctuations of the liquid alone.

Bessaid, B. S., Dellil, A. Z., Nemdili, F. and Azzi, A. (2017) [11]

The numerical simulation of turbulent thermal mixing in a rectangular T-junction, has been studied using the following models: SST-RANS, SST-URANS, and SST-SAS. It was noted that the SST-SAS model showed results similar to those obtained using LES simulation. While it is difficult for simulation using URANS approach to give the same results.

Bello, S. (2017) [12]

To study the effect between walls and liquid, treat the thermal shock and wall erosion, the code used for simulation in STAR-CCM. The first simulation: Changing the wall dimensions for a specific temperature in two mixing models. The second simulation: fixing the dimensions of the wall and changing the temperature in the entrance.

Cândido, S. and Páscoa, J. (2020) [13]

Investigated the impact of two specific turbulence models on calculating a mixture of gas-gas, using a 3D T-junction geometry. The differences between two RANS based model, the kw-SST and SAS were investigated.

Luaibi, M. S. and Abdulwahid, M. A. (2021) [14]

Used the stander k-ε model of turbulent in ANSYS FLUENT, to study the effect of the flow rate ratio with different Reynolds numbers in the range (3000-30000). The results show the loss coefficient is independent of the Re numbers.

Evrim, C. (2021) [15]

The LES is simulated for the horizontal and vertical flow with a flow ratio of 3 and a temperature range of 180°C in three different states depending on the position of the T-junction. First case: warm horizontal main pipe flow and a cold branch pipe flow coming from the side. The second case: warm horizontal main pipe flow and a cold branch pipe flow coming from vertical. Third case: warm horizontal main pipe flow and a cold branch pipe flow coming from above. Where the results were compared to the experimental data, the results showed different patterns of flow depending on the situation. In the first case, thermal mixing occurs in the lower part of the mixing zone with a stable laminar flow and the upper part remains warm, which is similar to the third case, while the mixing improved in the second case where the liquid was discharged over the entire cross section. Similar to the case, the increase in the Reynolds number contributes to the increase in the mixing of thermal fluctuations at the walls in the T-junction, and this is due to the shift and rotation of the thermal layers near the wall.

Luaibi, M. S. and Abdulwahid, M. A. (2022) [16]

Study of the flow dynamics at the T-junction and the prediction of the pressure loss factor in two cases (non-symmetrical dividing and non-symmetrical combining), the angle of the tee is 90º, sharp edge, the area ratio is equal to one and three-dimensional the specification of geometry at steady state, the model of turbulent uses the stander k-ε. The numerical results were compared to the effect of the flow ratio in the range of Reynolds number 3000-30000, where the results showed that the pressure loss coefficient is independent of the Reynolds number. The non-symmetrical dividing the maximum flow move in the straight pipe when the change flow rate ratio to (0.8) forced the fluid to move in the branch and formation high vortex and recirculation. The nonsymmetrical combining the high velocity in outlet branch with small eddies especially increased at a flow rate ratio (0.8).

CHAPTER 2:

TURBULENCE MODELING

Introduction:

In this chapter, one present a discussion about the various methods of modeling in turbulence simulation and computational fluid dynamics, and discuss some models for studying turbulence such as ($k-\varepsilon, k-\omega, and\ k-\omega-sst$). The Navier-Stokes equations for controlling turbulence are given.

2.1 Turbulence:

Despite the complexity and the equations for which we did not find an accurate solution to describe the turbulent, I do not say that it is impossible to define and predict the turbulence accurately, but it has become possible to get a very close idea about the behavior and characteristics of the turbulence, thanks to the efforts made in studying it by Engineers and researchers, as well as the development in differential equations modeling and computers, which have become much more powerful than they were previously. Nevertheless, challenges remain to reach a more and deeper understanding of the turbulence of flow in fluid mechanics. **[17]**

Experimental data was adopted and compared with the CFD simulation to find out the accuracy and knowledge reached by the researchers. But it is difficult to come up with a solution and a model that describes the turbulence in general, as turbulence occurs in various places, for example in nature, in the flow of rivers and seas and the flow of blood in the veins and the movement of winds and clouds, as well as in industrial places such as smoke from aircraft engines and at turbine blades and combustion inside engines, so the turbulence is a general type of medium flow and large size and varies according to different conditions, such as external flow, flow around the wing of the plane and around the cooling pipes, and internal such as flow inside a tube or a closed volume such as the combustion chamber in engines. **[18]**

Fig 1- Turbulence from aircraft swirling clouds [19].

2.1.1 Characteristics of turbulence:

- The unstable and irregular nature makes the turbulence follow many possibilities and methods and has forced us to follow the statistical or conditional way of describing it
- The nature of diffusion helps to mix well and quickly, which leads to resorting to most equations in fluid mechanics, such as the transfer of energy, mass and momentum
- Turbulence occurs when kinetic energy force dominates the force of viscosity, that is, a rise in the Reynolds number.
- The smallest scales of motion of turbulent flow are greater than the partial length, so the turbulent flow has no discontinuity, but is controlled by continuous mathematical equations.
- The movement of the turbulence is three-dimensional rotation and has more fluctuations than the fluctuations of the vortex, as the turbulence is unstable and does not maintain itself if the speed fluctuations are two-dimensional
- The characteristic of turbulent flow is dispersion, where the viscous shear stresses forces between the plates convert part of the kinetic energy of the turbulence into heat. **[20]**

2.2 Computational Fluid Dynamics:

It is the use of mathematics, physics and computer programs to predict and visualize how a gas or liquid flows, as well as how a gas or liquid affects. It is based mainly on Navier-Stokes equations that describe the relationship of various properties of liquid such as speed, temperature and density with each other. **[21]**

Computational fluid mechanic appeared in the early 20^{th} century and was known to most people as a tool for studying air flow around cars and airplanes and creating complex designs for cooling server rooms, and it became useful in studying heat flow and turbulent flow modeling. Flow characteristics to create a three-dimensional mathematical model on a grid that can be viewed and rotated from different angles, CFD can identify hot and sensitive areas and identify areas where energy waste or air mixing occurs. **[22]**

2.2.1 Phases of the CFD analysis:

- ***Pre-processing:*** At this stage, the problem information is transformed into a separate formal model in computer, and determined the type of flow to be designed (viscous/inviscid, compressible/incompressible, steady/non steady), and the other operations are mesh generation and the initial and applied boundary conditions.
- ***Solving:*** At this stage, the actual calculations are made in the analyzer, where computer power and good model selection and accuracy are required

- ***Post-processing:*** Finally, in this stage, the data is extracted and presented, where the analyst can verify the results, analyze them, and obtain conclusions based on them, and there are different ways to display the results such as graphs, images, animations in the form of videos, or tables. **[23]**

2.2.2 Field of use of the CFD simulation:

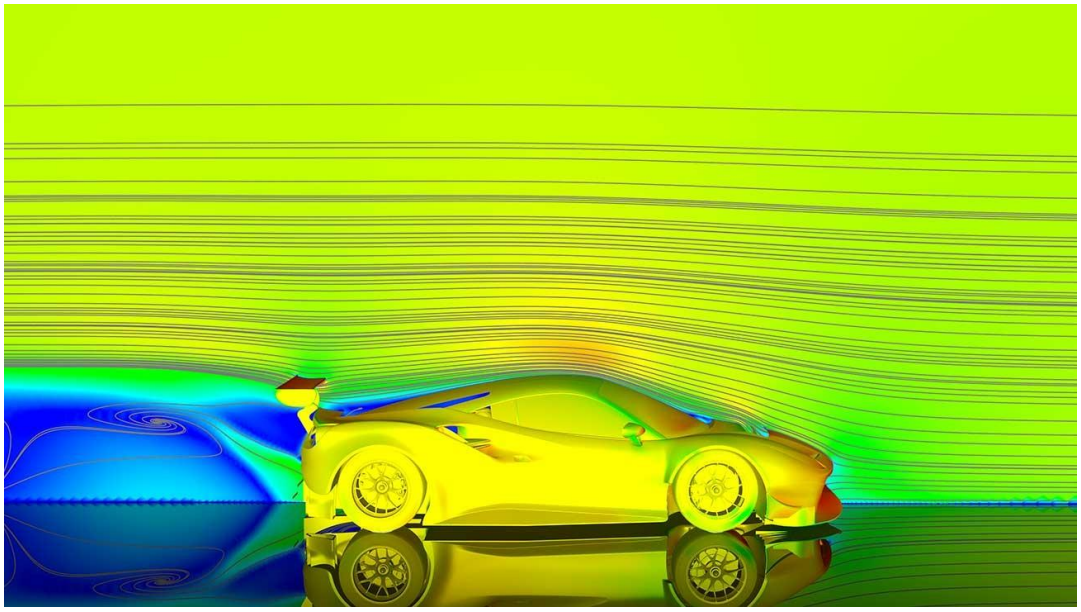

Fig 2- **CFD Simulation of a car [25].**

The field of use of the CFD simulation includes all phenomena that include fluid flow. Most of the important areas are [24]:

- For Preventing Cavitation
- Rotating Machinery using CFD
- Laminar and Turbulent Flow
- Heating, Air conditioning, and Ventilation (HVAC)
- Battery Simulation
- Aerodynamics
- Heat Transfer and Thermal Management
- Pipe and Valve
- Simulating Electronics Cooling
- Turbomachinery
- High Rheology Material
- Simulating Reacting Flows and Combustion
- Incompressible and Compressible Flow

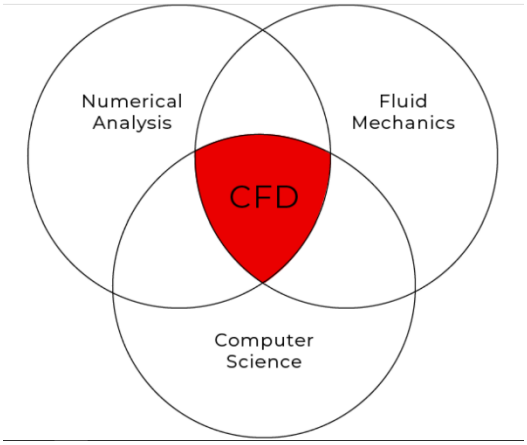

Fig 3- **Component domains of CFD [26]**

CFD simulations give us qualitative and quantitative predictions of fluid flow through:

- ❖ Mathematical equations for fluid dynamics and heat transfer
- ❖ Numerical methods (Mathematical Equation Modeling)
- ❖ Computer numerical processing (Using computer programs to perform the calculation, display and analyze the results)

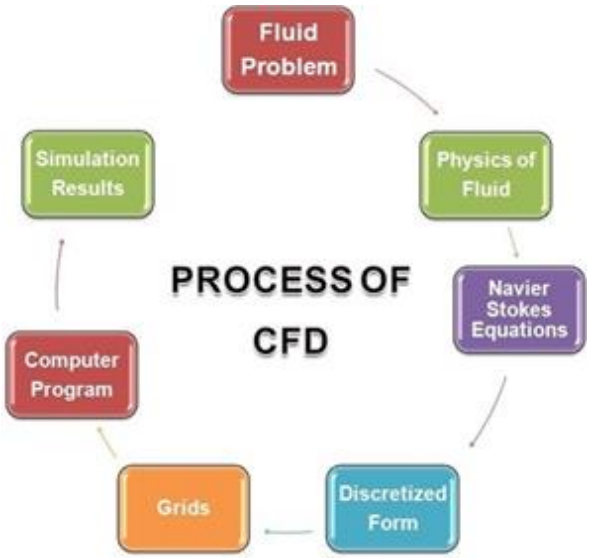

Fig *4* - Process of Computational Fluid dynamics [27].

2.3 Equations of Navier-Stokes:

The Navier-Stokes equation is a nonlinear partial differential equation that describes the motion of fluids in a continuous field.

It is possible to derive from it the equations that describe the various properties of the fluid motion, the equation of mass, energy and momentum. **[28]**

Continuity equation

$$\frac{\partial U_i}{\partial x_i} = 0 \qquad (1)$$

Momentum Equation

$$\underbrace{\rho \frac{\partial U_j}{\partial t}}_{\text{I}} + \rho \underbrace{U_i \frac{\partial U_j}{\partial x_i}}_{\text{II}} = \underbrace{-\frac{\partial P}{\partial x_j}}_{\text{III}} \underbrace{-\frac{\partial \tau_{ij}}{\partial x_i}}_{\text{IV}} + \underbrace{\rho g_j}_{\text{V}} \qquad (2)$$

Where

$$\tau_{ij} = -\mu\left(\frac{\partial U_j}{\partial x_i} + \frac{\partial U_i}{\partial x_j}\right) + \frac{2}{3}\delta_{ij}\mu\frac{\partial U_k}{\partial x_k} \qquad (3)$$

I: Local change with time

II: Momentum convection

III: Surface force

IV: Molecular dependent momentum exchange (diffusion)

V: Mass force

Energy Equation:

$$\underbrace{\rho c_\mu \frac{\partial T}{\partial t}}_{\text{I}} + \underbrace{\rho c_\mu U_i \frac{\partial T}{\partial x_i}}_{\text{II}} = \underbrace{-P\frac{\partial U_i}{\partial x_i}}_{\text{III}} + \underbrace{\lambda \frac{\partial^2 T}{\partial {x_i}^2}}_{\text{IV}} - \underbrace{\tau_{ij}\frac{\partial U_j}{\partial x_i}}_{\text{V}} \qquad (4)$$

I: Local energy change with time

II: Convective term

III: Pressure work

IV: Heat flux (diffusion)

V: Irreversible transfer of mechanical energy into heat

2.4 Modeling methods:

Mostly the flows are turbulent, so we have to solve these disturbances most of the time, and to get correct and reliable results we have, to model the turbulence.

The figure below represents a diagram that summarizes the most common methods for solving turbulent flows, as the time cost and quality of devices used in the simulation increase from RANS to DNS with other factors such as increasing the degree of freedom to resolve turbulent flow, and since the computational costs of LES and DNS are large, it is a simulation used in Academic studies are intended for scientific research, and are applied to simple shapes and have a rather small and medium size, while to solve industrial problems and problems that require urgent solutions, the use of RANS-LES, URANS and RANS methods is the best and option. **[29]**

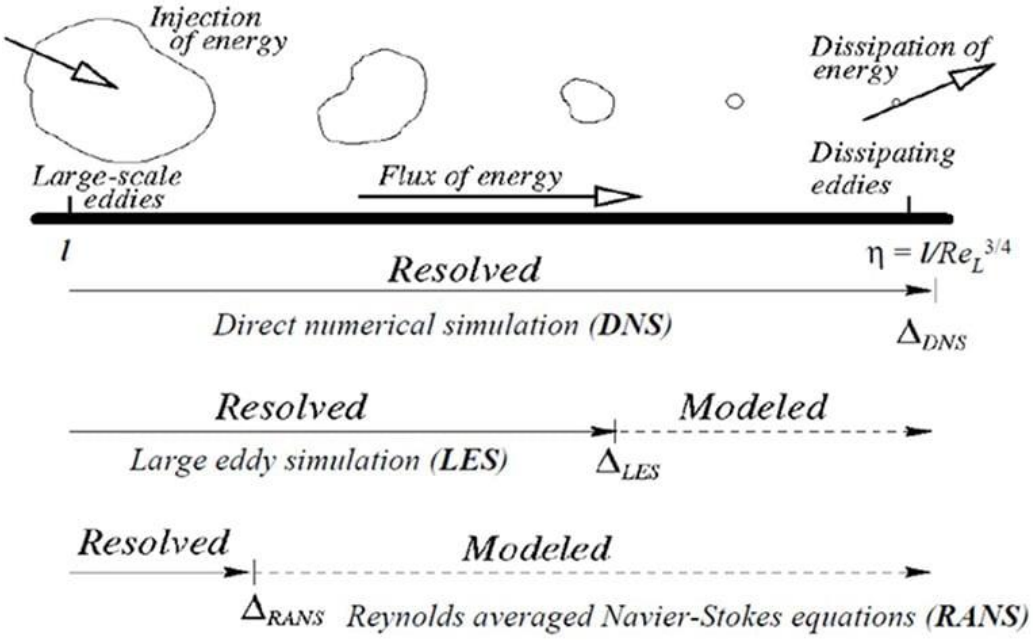

Fig *5*- **Turbulence models in CFD from RANS to DNS. [30]**

2.4.1 Reynolds Averaged Navier-Stokes (RANS):

It presents statistical results and average values after performing statistical calculations in the Navier-stokes equation, and it does not provide small and accurate results, but rather results that show the general shape of the flow over a time domain. This method does not require complex methods for solving and mesh, and it is used recently to save time and reduce experimental tests as much as possible, in the RANS approach, there is no unified model for the calculation, but there are several models that require good selection according to the case studied to obtain more accurate results. **[31]**

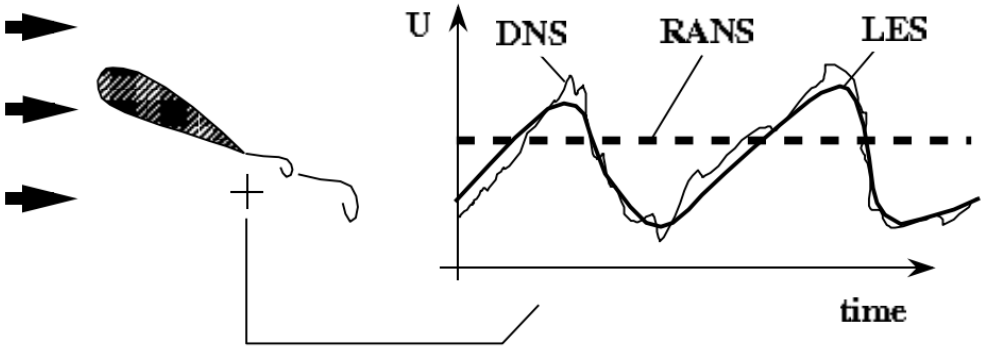

Fig 6- **Principle of the DNS, LES and RANS approaches. [31]**

And recently, this is the most common and widely used method to bypass time-wasting and costly tests. All that is required is the modeling of the basic nonlinear equations in fluid dynamics and the averaging of the various values that characterize the studied turbulent flow. In industrial applications, we find that the most widely used method is RANS, or URANS depending on the characteristics of the turbulent flow.

Due to the complex applications in turbulence simulation and the nature of small turbulence, the RANS approach provides comprehensive and similar flow structures that do not allow us to observe the details and small fluctuation of the flow, while the LES approach provides the term pressures for sub-grid measures, which are not present in the RANS approach. **[32]**

2.4.2 Large Eddy Simulation (LES):

The LES simulation mediates between the RANS approach and the DNS approach. It includes the technique of statistical computation, presenting results as average values, and true and accurate computation, and this depends on the size of the scales we want to calculate. It is not affected by the flow significantly, so it tends to model these small sizes, as for the large domain sizes, they are calculated with accuracy based on the DNS approach, and we can say that the LES approach provides an accurate study with a significant saving of time and data volume compared to the DNS approach and also considered as a modifier of the DNS approach with fluctuations that cannot be neglected in order to obtain a careful and in-depth study. **[33]**

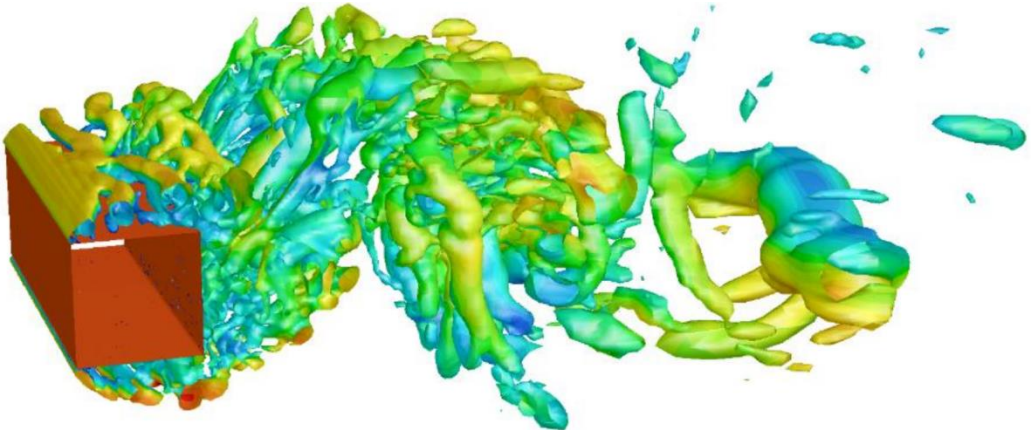

Fig *7* – "LES" simulation of a fluid flowing on a cuboid. [34]

2.4.3 Hybrid RANS-LES model (DES):

To take advantage of the simulation using RANS and LES, they are combined into a single approach called RANS-LES to mitigate the significant cost of the LES approach while maintaining computational efficiency.

We often find the accuracy of the grid focused on surfaces and important objects as is the case in LES, and this requires calculating the flow accurately near surfaces and objects, and in order to be able to perform the calculations at a rather low cost compared to LES we had to reduce the accuracy of the grid near the walls where it is used an hybrid method of computation called Detached Eddy Simulation (DES), is based on the use of RANS near the wall and LES away from the walls, as it removes some of the limitations of the RANS approach and provides more accurate and clear results that we can rely on in complex and unstable flows, where the Accuracy and in-depth and detailed study are important. **[32]**

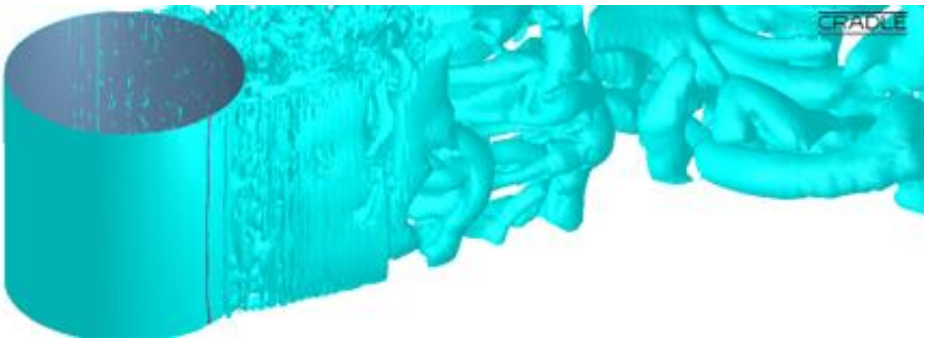

Fig *8* – "DES" simulation of a cylinder above a surface. [35]

2.4.4 Direct Numerical Simulation (DNS):

In the direct numerical simulation (DNS), the flow parameters are calculated using the Navir-stokes equations spatially and temporally with high accuracy, and in the early 1970s, the low dissipation and dispersion errors methods were frequently relied upon to simulate turbulent flows, and in the first applications, the DNS simulation was used in a direct way, but with the presence of complex geometric shapes and process flows, there was a need to create effective diagrams to deal with them, as methods of spectral elements were developed to deal with these complex shapes. **[36]**

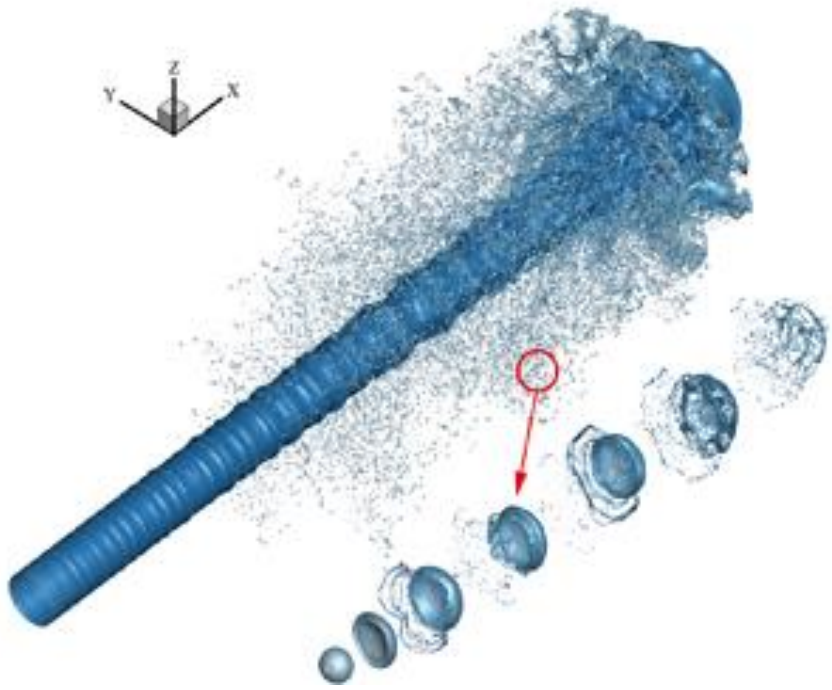

Fig *9* **- "DNS" simulation of a liquid jet [37]**

2.5 Turbulence model:

2.5.1 k − ε Model:

To date, the $k-\varepsilon$ model is the most common and widely used, and the first to work on and develop this model were Chou (1945), Davidov (1961) and Harlow and Nakayama (1968). With the developments in computer technology in the early seventies, the great use of this model began after the release of Jones and Launder (1972), and in 1974 Launder and Sharma worked on modifying the closure coefficient of the model, which is the model referred to as the standard $k-\varepsilon$ model. **[38]**

The quantity ε is the dissipation per unit mass and is defined by the following correlation.

$$\varepsilon = \nu \overline{\frac{\partial u_i'}{\partial x_k}\frac{\partial u_i'}{\partial x_k}} \tag{5}$$

We begin with Equation (6)

$$\frac{\partial k}{\partial t} + U_j\frac{\partial k}{\partial x_j} = \tau_{ij}\frac{\partial U_i}{\partial x_j} - \varepsilon + \frac{\partial}{\partial x_j}\left[(\nu + \nu_T/\sigma_k)\frac{\partial k}{\partial x_j}\right] \tag{6}$$

Where τ_{ij} is Reynolds-stress tensor

$$\tau_{ij} = 2\nu_T S_{ij} - \frac{2}{3}k\delta_{ij} \tag{7}$$

The exact equation for ε is derived by taking the following moment of the Navier-Stokes equation:

$$\varepsilon = \nu \overline{\frac{\partial u_i'}{\partial x_j}\frac{\partial}{\partial x_j}[N(u_i)]} \tag{8}$$

Where $N(u_i)$ is the Navier-Stokes operator

$$N(u_i) = \rho\frac{\partial u_i}{\partial t} + \rho u_k\frac{\partial u_i}{\partial x_k} + \frac{\partial p}{\partial x_i} - \mu\frac{\partial^2 u_i}{\partial x_k \partial x_k} \tag{9}$$

After a considerable amount of algebra, the following exact equation for ε results.

$$\frac{\partial \varepsilon}{\partial t} + U_i\frac{\partial \varepsilon}{\partial x_j} = -2\nu\left[\overline{u_{\iota,k}'u_{j,k}'} + \overline{u_{k,\iota}'u_{k,J}'}\right]\frac{\partial U_i}{\partial x_j} - 2\nu\,\overline{u_k'u_{\iota,J}'}\frac{\partial^2 U_i}{\partial x_k \partial x_j} - 2\nu\,\overline{u_{\iota,k}'u_{\iota,m}'u'_{k,m}}$$
$$- 2\nu^2\overline{u_{\iota,km}'u_{\iota,km}'} + \frac{\partial y}{\partial x}\left[\nu\frac{\partial y}{\partial x} - \nu\overline{u'_J u'_{\iota,m}u'_{\iota,m}} - 2\frac{\nu}{\rho}\overline{p'_{,m}u'_{J,m}}\right] \tag{10}$$

The complex form of the equation ε prevents us from using it in simple models, and in order to exclude this problem, Harlow and Nakayama (1968) and Hanjalic (1970) proposed a hypothesis that states that ε has the same form as the turbulent kinetic energy equation. **[33]**

The standard k-ε is as follows:

Kinematic Eddy Viscosity:

$$\nu_T = {C_\mu k^2}/{\varepsilon} \tag{11}$$

Turbulence Kinetic Energy:

$$\frac{\partial k}{\partial t} + U_j\frac{\partial k}{\partial x_j} = \tau_{ij}\frac{\partial U_i}{\partial x_j} - \varepsilon + \frac{\partial}{\partial x_j}\left[(\nu + \nu_T/\sigma_k)\frac{\partial k}{\partial x_j}\right] \tag{12}$$

Dissipation Rate:

$$\frac{\partial \varepsilon}{\partial t} + U_j \frac{\partial \varepsilon}{\partial x_j} = C_{\varepsilon 1} \frac{\varepsilon}{k} \tau_{ij} \frac{\partial U_i}{\partial x_j} - C_{\varepsilon 2} \frac{\varepsilon^2}{k} + \frac{\partial}{\partial x_j} \left[(\nu + \nu_T / \sigma_\varepsilon) \frac{\partial \varepsilon}{\partial x_j} \right] \quad (13)$$

Closure Coefficients and Auxiliary Relations: [33]

$$C_{\varepsilon 1} = 1.44, \qquad C_{\varepsilon 2} = 1.92, \qquad C_\mu = 0.09, \qquad \sigma_k = 1.0, \qquad \sigma_\varepsilon = 1.3$$

$$\omega = {\varepsilon}/{C_\mu k} \ , \ \ell = {C_\mu k^{3/2}}/{\varepsilon}$$

The k-ε model has been updated by Yakhot and Orszag (1986) [see also Yakhot et al. (1992)] and this is by using the renormal-ization group theory, where the role of the equations (11), (12) and (13) remains the same to calculate the eddy viscosity, k and ε with the updated coefficient $C_{\varepsilon 2}$ defined by:

$$C_{\varepsilon 2} \equiv \tilde{C}_{\varepsilon 2} + \frac{C_\mu \lambda^3 (1 - \lambda/\lambda_0)}{1 + \beta \lambda^3} \qquad , \qquad \lambda \equiv \frac{k}{\varepsilon} \sqrt{2 S_{ij} S_{ji}}$$

The closure coefficients for the RNG $k - \varepsilon$ model are

$$C_{\varepsilon 1} = 1.42 \ , \ \tilde{C}_{\varepsilon 2} = 1.68 \ , \ C_\mu = 0.058 \ , \ \sigma_\varepsilon = 0.72 \ , \ \sigma_k = 0.72$$

$$\beta = 0.012 \quad , \ \lambda_0 = 4.38$$

2.5.2 $k - \omega$ Model:

The first model of the dual turbulence equation was in 1942 by Kolmogorov, where he formulated the kinetic energy equation for the turbulence to describe the turbulent flow. The equation showed the dissipation factor of the kinetic energy of the turbulence per unit kinetic energy of the disturbance ω, is relative and its differential equation is similar to the differential equation for $\boldsymbol{k}$ and ε In 1970, Saffman presented a model that is characterized by its accuracy from the Kolmogorov model, while Spalding removed some defects in the Kolmogorov model, where he presented an improved version of it.

After that, attention focused on this model, and work continued on it, and improvements appeared in a time domain that corresponds to the development in computers [Wilcox and Alber (1972), Saffman and Wilcox (1974), Wilcox and Traci (1976), Wilcox and Rubesin (1980), Wilcox (1988a) and Wilcox (1998)]. **[32]**

Kolmogorov realized that the feature of unstable fluid motion showed that our equations were insufficient to describe it, so he combined kinetic energy dissipation rates and kinetic energy generation and dimensional analyzes, where he hypothesized the form of the ω equation with the intent of closing the Navier-Stokes system of equations and calculating it

$$\frac{\partial \omega}{\partial t} + U_j \frac{\partial \omega}{\partial x_j} = -\beta \omega^2 + \frac{\partial}{\partial x_j} \left[\sigma \nu_T \frac{\partial \omega}{\partial x_j} \right] \qquad (14)$$

The prediction accuracy of Wilcox (1988a) model in the free shear and discrete flows has been greatly increased with the advent of the next version of the k − ω model. **[32]**

Kinematic Eddy Viscosity:

$$\nu_T = \frac{k}{\widetilde{\omega}} \qquad (15)$$

$$\widetilde{\omega} = max\left\{\omega, C_{lim}\sqrt{\frac{2S_{ij}S_{ij}}{\beta^*}}\right\} \ , \quad C_{lim} = \frac{7}{8}$$

Turbulence Kinetic Energy:

$$\frac{\partial k}{\partial t} + U_j\frac{\partial k}{\partial x_j} = \tau_{ij}\frac{\partial U_i}{\partial x_j} - \beta^* k\omega + \frac{\partial}{\partial x_j}\left[\left(\nu + \sigma^*\frac{k}{\omega}\right)\frac{\partial k}{\partial x_j}\right] \quad (16)$$

Specific Dissipation Rate:

$$\frac{\partial \omega}{\partial t} + U_j\frac{\partial \omega}{\partial x_j} = \alpha\frac{\omega}{k}\tau_{ij}\frac{\partial U_i}{\partial x_j} - \beta\omega^2 + \frac{\sigma_d}{\omega}\frac{\partial k}{\partial x_j}\frac{\partial \omega}{\partial x_j} + \frac{\partial}{\partial x_j}\left[\left(\nu + \sigma\frac{k}{\omega}\right)\frac{\partial \omega}{\partial x_j}\right] \quad (17)$$

Closure Coefficients and Auxiliary Relations:

$$\alpha = \frac{13}{25}, \qquad \beta = \beta_0 f_\beta, \qquad \beta^* = \frac{9}{100}, \qquad \sigma = \frac{1}{2}, \qquad \sigma^* = \frac{3}{5}, \qquad \sigma_{do} = \frac{1}{8}$$

$$\sigma_d = \begin{cases} 0, & \frac{\partial k}{\partial x_j}\frac{\partial \omega}{\partial x_j} \le 0 \\ \sigma_{do}, & \frac{\partial k}{\partial x_j}\frac{\partial \omega}{\partial x_j} > 0 \end{cases}$$

$$\beta_0 = 0.0708 \ , \ f_\beta = \frac{1 + 85\chi_\omega}{1 + 100\chi_\omega} \ , \ \chi_\omega \equiv \left|\frac{\Omega_{ij}\Omega_{jk}S_{ki}}{(\beta^*\omega)^3}\right|$$

$$\varepsilon = \beta^*\omega k \ , \ \ell = {k^{1/2}}/{\omega}$$

We refer to all equations as the Wilcox (2006) $k - \omega$ model.

Tensors Ω_{ij} and S_{ij} are the mean-rotation and mean-strain-rate tensors, respectively defined by:

$$\Omega_{ij} = \frac{1}{2}\left(\frac{\partial U_i}{\partial x_j} - \frac{\partial U_j}{\partial x_i}\right) \ , \ S_{ij} = \frac{1}{2}\left(\frac{\partial U_i}{\partial x_j} + \frac{\partial U_j}{\partial x_i}\right)$$

2.5.3 $k - \omega$ - SST Model:

The $SST\ k - \omega$ turbulence model is two-equation eddy viscosity model [Shear Stress Transport-Menter 1993] that is widely used recently because of its features that combine two models that cover with some geometric field of the flow, whether it is near the wall or away from it, as we find it behaves k-ω in the boundary layer adjacent to the wall, $k - \varepsilon$ behaves in free flows away from the walls, avoiding sensitivity to low pressure gradients and discrete flows, this enables it to accurately predict the separation zones in flows with non-flat surfaces such as those used in aerodynamics. **[38]**

Kinematic Eddy Viscosity:

$$\nu_T = \frac{a_1 k}{max(a_1\omega, SF_2)} \quad (18)$$

$\boldsymbol{F_2}$ (Second blending function)

$$F_2 = tanh\left[\left[\max\left(\frac{2\sqrt{k}}{\beta^*\omega y}, \frac{500\nu}{y^2\omega}\right)\right]^2\right] \quad (19)$$

Turbulence Kinetic Energy:

$$\frac{\partial k}{\partial t} + U_j\frac{\partial k}{\partial x_j} = P_k - \beta^* k\omega + \frac{\partial}{\partial x_j}\left[(\nu + \sigma_k\nu_T)\frac{\partial k}{\partial x_j}\right] \quad (20)$$

$\boldsymbol{P_k}$ (Production limiter)

$$P_k = min\left(\tau_{ij}\frac{\partial U_i}{\partial x_j}, 10\beta^* k\omega\right) \quad (21)$$

Specific Dissipation Rate:

$$\frac{\partial \omega}{\partial t} + U_j\frac{\partial \omega}{\partial x_j} = \alpha S^2 - \beta\omega^2 + \frac{\partial y}{\partial x}\left[(\nu + \sigma_\omega\nu_T)\frac{\partial \omega}{\partial x_j}\right] + 2(1 - F_1)\sigma_{\omega^2}\frac{1}{\omega}\frac{\partial k}{\partial x_i}\frac{\partial \omega}{\partial x_i} \quad (22)$$

$\boldsymbol{F_1}$ (Blending Function)

$$F_1 = tanh\left\{\left\{min\left[max\left(\frac{\sqrt{k}}{\beta^*\omega y}, \frac{500\nu}{y^2\omega}\right), \frac{4\sigma_{\omega^2}k}{CD_{k\omega}y^2}\right]\right\}^2\right\} \quad (23)$$

Where $CD_{k\omega}$ define by

$$CD_{k\omega} = max\left(2\rho\sigma_{\omega 2}\frac{1}{\omega}\frac{\partial k}{\partial x_i}\frac{\partial \omega}{\partial x_i}, 10^{-10}\right) \quad (24)$$

Note*:* $F_1 = 1$ inside the boundary layer and 0 in the free stream. And y is the closest distance to the wall.

Closure Coefficients and Auxiliary Relations:

All constants are calculated by mixing the corresponding constants of the model k - ε and model k–ω by:

$$\alpha = \alpha_1 F_1 + \alpha_2(1 - F_1) \quad (25)$$

Avec:

$$\alpha_1 = \frac{5}{9}, \quad \alpha_2 = 0.44, \quad \beta_1 = \frac{3}{40}, \quad \beta_2 = 0.0828, \quad \beta^* = \frac{9}{100}$$

$$\sigma_{k1} = 0.85, \quad \sigma_{k2} = 1, \quad \sigma_{\omega 1} = 0.5, \quad \sigma_{\omega 2} = 0.856$$

CHAPTER 3: NUMERICAL RESOLUTION AND FREE SOFTWARES

Introduction

An introduction and the advantages of the open source and free CFD software (Code_Saturne, Salome and ParaView), are presented. A presentation an also of the free software Grace, which is a 2D graphics drawing tool.

3.1 Presentation of Salome:

Salome is a free and open-source CAD program. It is easy to deal with since it contains everything the simulation requires, from creating the engineering model to displaying the data and results. It was developed according to the participants in the development of the program.

Salome software is used to generate the geometry and the mesh.

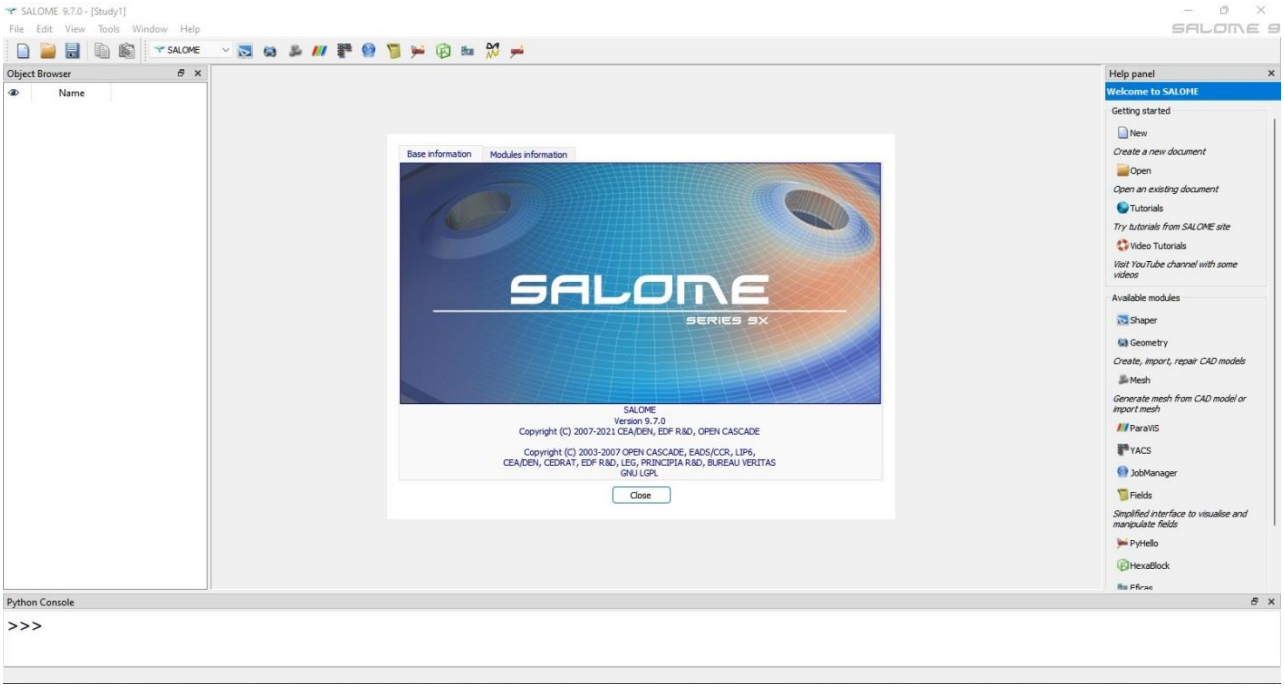

Fig *10* - Salome graphical interface.

3.2 Code_Saturne Software:

Code_Saturne is a program used to perform computational simulations to solve fluid dynamics applications developed and released by EDF. The code is **free** and **open-source**.

The program models Navier-Stokes equations for two-dimensional or three-dimensional flows with various flow patterns, whether laminar or turbulent, as well as with various physical properties of extensibility, and customizes the flow such as isothermal flow or not.

The models in this program vary, such as the Reynolds-Averaged (RANS) and Large-Eddy Simulation model (LES), while providing updates in line with the developments that occur in the field of numerical simulation. It also contains models for the effects of specific physical phenomena such as: gas, coal and heavy-fuel oil combustion, semi-transparent radiative transfer,

particle-tracking with Lagrangian modeling, Joule effect, electrics arcs, weakly compressible flows, atmospheric flows, rotor/stator interaction for hydraulic machines. **[39]**

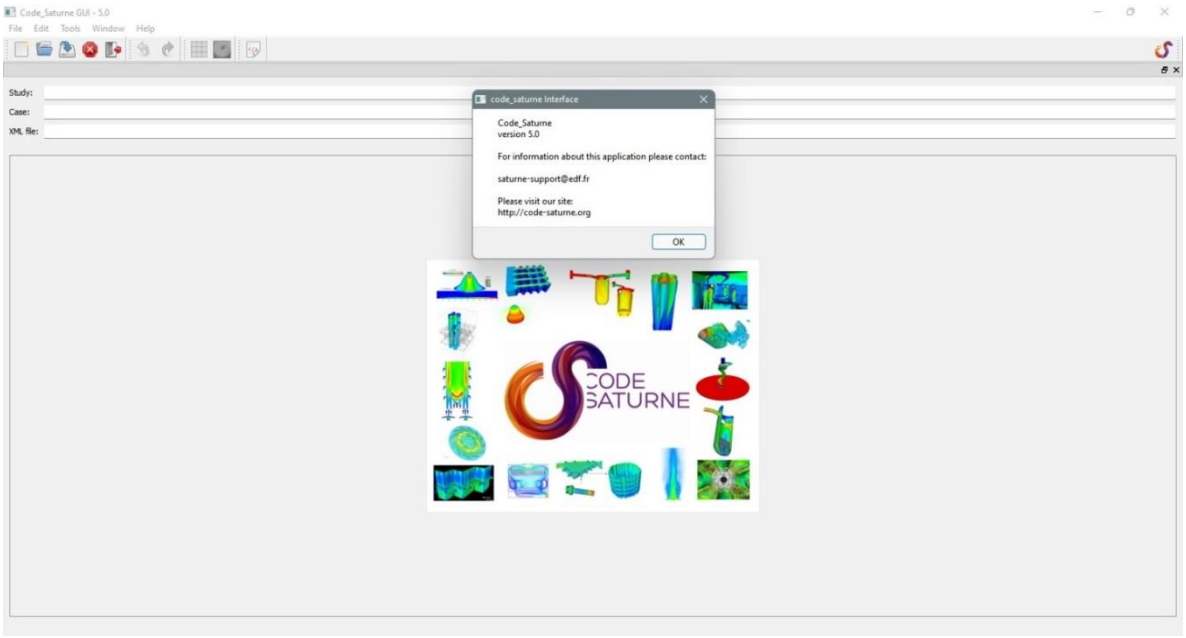

Fig *11*- Code_Satunre graphical interface

3.2.1 Numerical method:

Discretization

Code_Saturne is based on a co-located Finite Volume approach that handles meshes with any type of cell (tetrahedral, hexahedral, prismatic, pyramidal, polyhedral…) and any type of grid structure (unstructured, block structured, hybrid, conforming or with hanging nodes…).

Code_Saturne can solve flows in steady or unsteady mode. It uses a theta scheme for the time discretization. **[37]**

Velocity-pressure coupling

- Code_Saturne uses a fractional step method, similar to SIMPLEC.
- Velocity prediction: Solve the momentum equation with an explicit pressure gradient and obtain a predicted velocity
- Pressure correction: Use the continuity equation to enforce mass conservation
- Update velocity field using ∇P
- After the velocity has been updated, the resolution of turbulent variables and scalars is done according to their time scheme. **[37]**
- Rhie & Chow interpolation is used when solving the pressure to avoid oscillations.

Linear system resolution

- *Code_Saturne* has different ways of solving the linear system:
- Jacobi (default for velocity, temperature, turbulent variables, passive scalars)
- Algebraic multigrid (default for pressure)
- Conjugate gradient
- Stabilized bi-conjugate gradient (BI-CGSTAB)

Convective scheme

- Different schemes for convective terms are available in *Code_Saturne*:
- First order Upwind Scheme
- Centered scheme
- Second Order Linear Upwind (SOLU) Scheme
- Blended scheme between upwind and second order scheme
- A slope test is activated by default for second order schemes to switch from second order to upwind in case of overshoots

Gradient calculation

- In *Code_Saturne* several options are available:
- Iterative reconstruction of the non-orthogonalities (initialization by zero or based on the least-square method)
- Least squares method (with a standard, extended or partial extended neighborhood)

3.3 Presentation of Paraview:

ParaView is an open-source multi-platform application designed to visualize data sets of different sizes from small to large. The goals of the ParaView project include the development of open source, multi-platform visualization applications that support distributed computing models to process large data sets. It has an open, flexible and intuitive user interface. In addition, ParaView is built on an extensible architecture based on open standards. ParaView runs on distributed and shared memory parallel and single-processor systems, and has been successfully tested on Windows, Linux, Mac OS X, IBM Blue Gene, Cray XT3 and various Unix workstations and clusters. At the bottom, ParaView uses a visualization toolkit as a data processing and rendering engine, and has a user interface written using the Qt cross-platform application framework. **[40]**

ParaView leverages parallel data processing and rendering to enable interactive visualization for extremely large datasets. It also includes support for large displays including tiled displays and immersive 3D displays with head tracking and wand control capabilities.

ParaView also supports scripting and batch processing using Python. Using included Python modules, you can write scripts that can perform almost all the functionality exposed by the interactive application and much more.

ParaView is open-source (BSD licensed, commercial software friendly). As with any successful open-source project, ParaView is supported by an active user and developer community. **[41]**

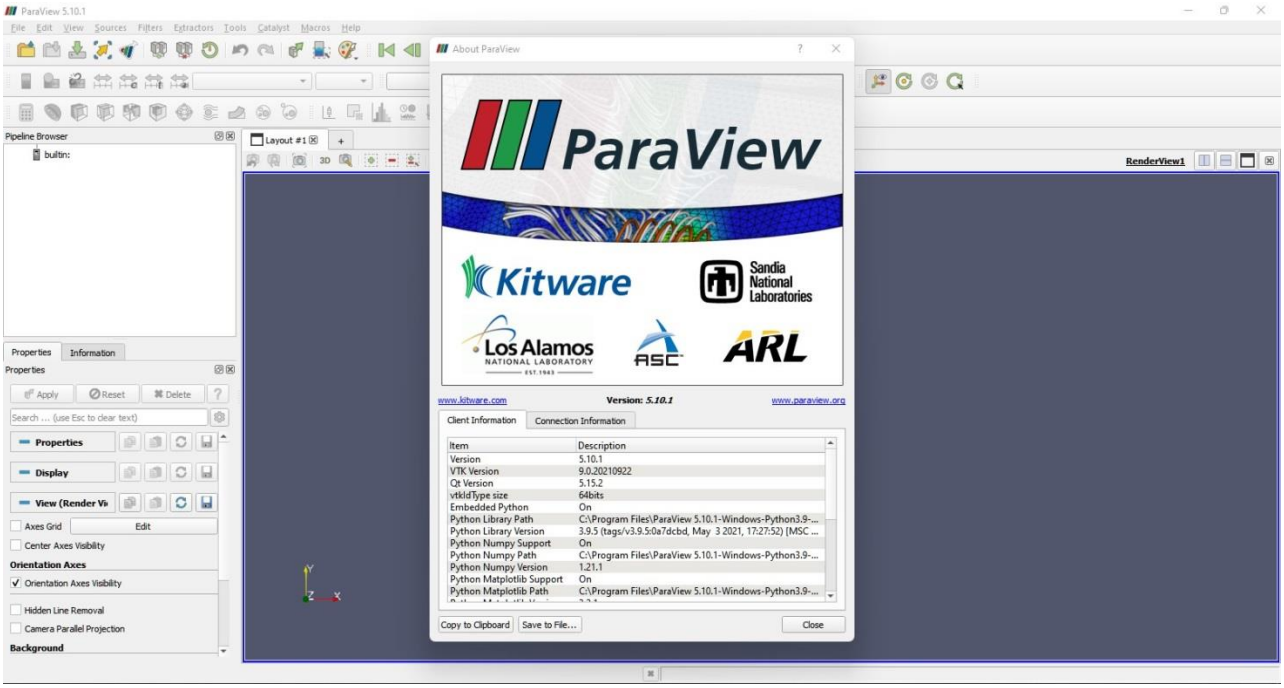

Fig *12*- **ParaView graphical interface**

3.4 Grace software:

Grace is a tool for making two-dimensional graphs of numerical data. Its functions are roughly similar to GUI-based programs such as Sigmaplot or Microcal Origin, and script-based tools such as gnuplot or Genplot. Its advantage is that it combines the convenience of a graphical user interface with the powerful functions of a scripting language, enabling it to perform complex calculations or perform automated tasks.

Grace is derived from Xmgr (aka ACE/gr) and was originally written by Paul Turner.

Starting from version 4.00, under the coordination of Evgeny Stambulchik, a team of volunteers took over the development work.

When its copyright was changed to GPL, its name was changed to Grace, which stands for "GRaphing, Advanced Computation and Exploration of data" or "Grace Revamps ACE/gr".**[42]**

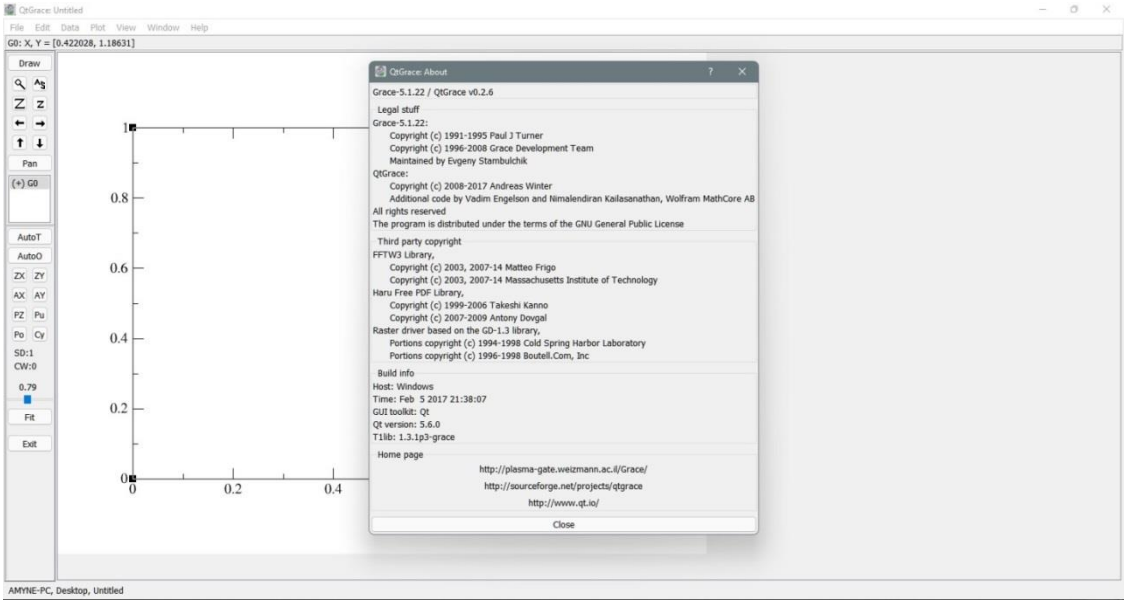

Fig *13*- PreView of QtGrace, showing the Fourier transforms dialogue

Note:

All the software used in these simulations are

‘’FREE’’ and some of them are ‘’OPEN SOURCE’’

CHAPTER 4:

STUDY CASE

Introduction:

Due to the presence configuration of the T-junction in industry and even nature, it has been studied and taken care of, as the simplified geometry of the T-junction made academic researchers use the simulation approach and computers with great power in simulation to check and study the obtained results.

In this chapter, the flow at the T junction is studied. A dynamic study with equal temperature for the two inputs, that is, a dynamic study with a thermal and dynamic study, to Code_Saturne calculation program is used accomplish this simulation.

4.1 Case study of the mixing T-junction:

Regardless of the rather simple geometry and mesh, T-junction flow is important research in CFD computational fluid dynamics, and has a complex flow nature that makes its calculations very difficult.

4.1.1 Geometry:

The geometry consists of a horizontal main inlet with a diameter of 140 mm and a length of 0.42 m to the center of the T junction, and a vertical secondary inlet whose direction of flow is the same as the direction of the gravitational ray with a diameter of 100 mm and a length of 0.31 m to the center of the T junction, and a horizontal outlet along the main inlet and The outlet diameter is the same as the main inlet diameter is 140 mm and its length from the center of the T intersection to the end is 3.08 meters.

We consider the origin of the three-dimensional landmark is the point of intersection of the two inlets, where the horizontal X axis parallels the main inlet (inlet_1) and outlet, and the Z axis is opposite the direction of the gravitational ray

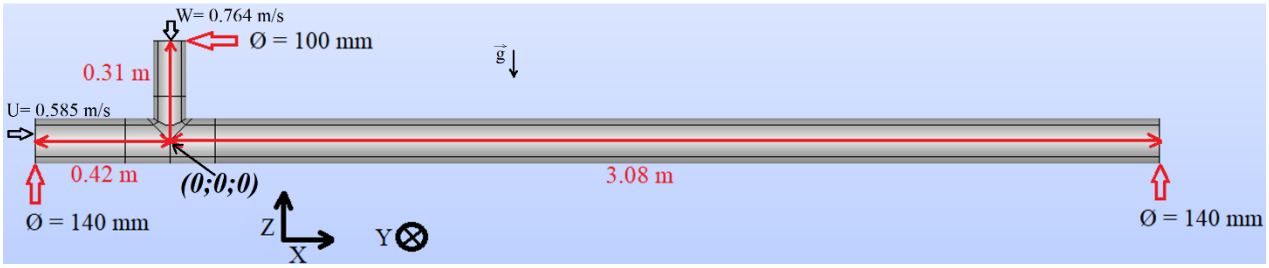

Fig *14*- Geometric dimensions of the T junction

A mesh sensitivity test with a comparison of four grids (magnified, medium, refined and over refined) was carried out, to define the best mesh to use for the next calculations.

Table 1- **Meshes with the number of cells**

Mesh	Coarse (a)	Medium (b)	Fine (c)	Very fine (d)
Nb. of cells	10368	23644	262520	602712

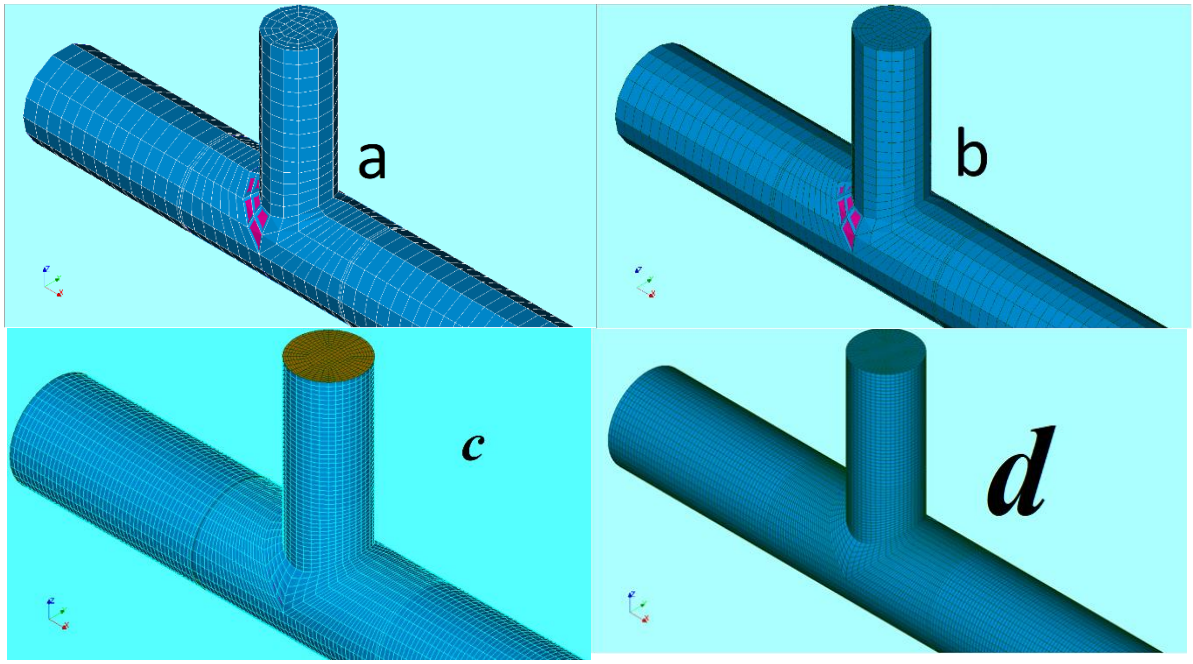

Fig *15*- **Zoom of the coarse (a), medium (b), fine (c) and very fine (d) mesh in the XZ plane for the configuration of a smooth cylinder.**

4.1.2 Physical parameters:

The fluid properties of the dynamic study are shown in the following table-2 **[5]**

Table 2- **The fluid properties at 25 C°**

T(◦C)	ρ(kg/m3)	k(W/mK)	μ(PA.s)	Cp(J/kg.K)	Pr(−)
25	997.2	0.6076	0.8904×10^{-3}	4179	6.125

The Reynolds number (Re) is used to determine whether the fluid flow is laminar or turbulent.

Internal Flow:

Table 3- **Flow regime by Re number**

Flow type	**Reynolds Number Range**
Transition regime	2300<Re<4000
Turbulent regime	Re>4000

And to make sure that the studied flow is a turbulent, we calculate the Reynolds number for the two inlets.

For main inlet (inlet_1):

$$Re_{In\_1} = \frac{\rho * U * D_{In\_1}}{\mu} \qquad (26)$$

$$Re_{In\_1} \approx \frac{997.2 * 0.585 * 0.14}{0.0008904}$$

$$Re_{In\_1} \approx 91723$$

For main inlet (inlet_2):

$$Re_{In\_2} = \frac{\rho * W * D_{In\_2}}{\mu} \qquad (27)$$

$$Re_{In\_2} \approx \frac{997.2 * 0.764 * 0.1}{0.0008904}$$

$$Re_{In\_2} \approx 85563$$

We note that the Reynolds number corresponds to the turbulent flow in both inputs.

For the thermal study of the mixing T-junction, we kept the same shape of the first part with a temperature at the main inlet (inlet_1) to 19 ° C and the temperature at the secondary inlet (inlet_2) to 36 ° C. The properties of the fluid are shown in the table (4), below.

Table 4-**The fluid properties at 20 C° and 35 C°**

T(◦C)	ρ(kg/m3)	k(W/mK)	μ(PA.s)	Cp(J/kg.K)	Pr(−)
20	998.3	0.5996	1.0020 x 10^{-3}	4182	6.988
35	994.1	0.6221	0.7196 x 10^{-3}	4178	4.833

The equations for the properties of the liquid are: **[43]**

$$C_p(T) = -1.0224\ 10^{-3}\ T^3 + 2.9201\ 10^{2}\ T^2 - 1.822\ T + 4209.9 \qquad (28)$$

$$\mu(T) = -1.9296\ 10^{-9}\ T^3 + 4.7256\ 10^{-7}\ T^2 - 4.2088\ 10^{-5}\ T + 1.6947\ 10^{-3} \qquad (29)$$

$$\frac{\lambda}{C_p(T)} = -3.0374\ 10^{-13}\ T^3 - 2.1701\ 10^{-9}\ T^2 - 4.7970\ 10^{-7}\ T + 1.3538\ 10^{-4} \qquad (30)$$

$$\rho(T) = 1.4078\ 10^{-5}\ T^3 - 5.5855\ 10^{-3}\ T^2 - 2.8886\ 10^{-3}\ T + 1000.4 \qquad (31)$$

CHAPTER 5: RESULTS AND DISCUSSION

Introduction

In this chapter, we will discuss and analyze the results obtained from the simulation process using the k - w - SST model, we consider reference temperature as $T_{ref} = \frac{T - T_{min}}{T_{max} - T_{min}}$ and we consider the diameter of the main pipe D = 0.14 m as the reference and the vertical flow velocity U = 0.585 m/s as the reference velocity in both parts, which are:

Dynamic simulation: where the temperature is fixed at 25 ° C, as well as the corresponding density and viscosity.

Thermal and dynamic simulation: where two flows of different temperature are mixed and the fluid properties functions are entered with the temperature change in the simulation program.

And we will compare the results obtained in the thermal and dynamic simulations with the experimental results.

5.1 First part: Dynamic simulation:

5.1.1 Sensitivity study:

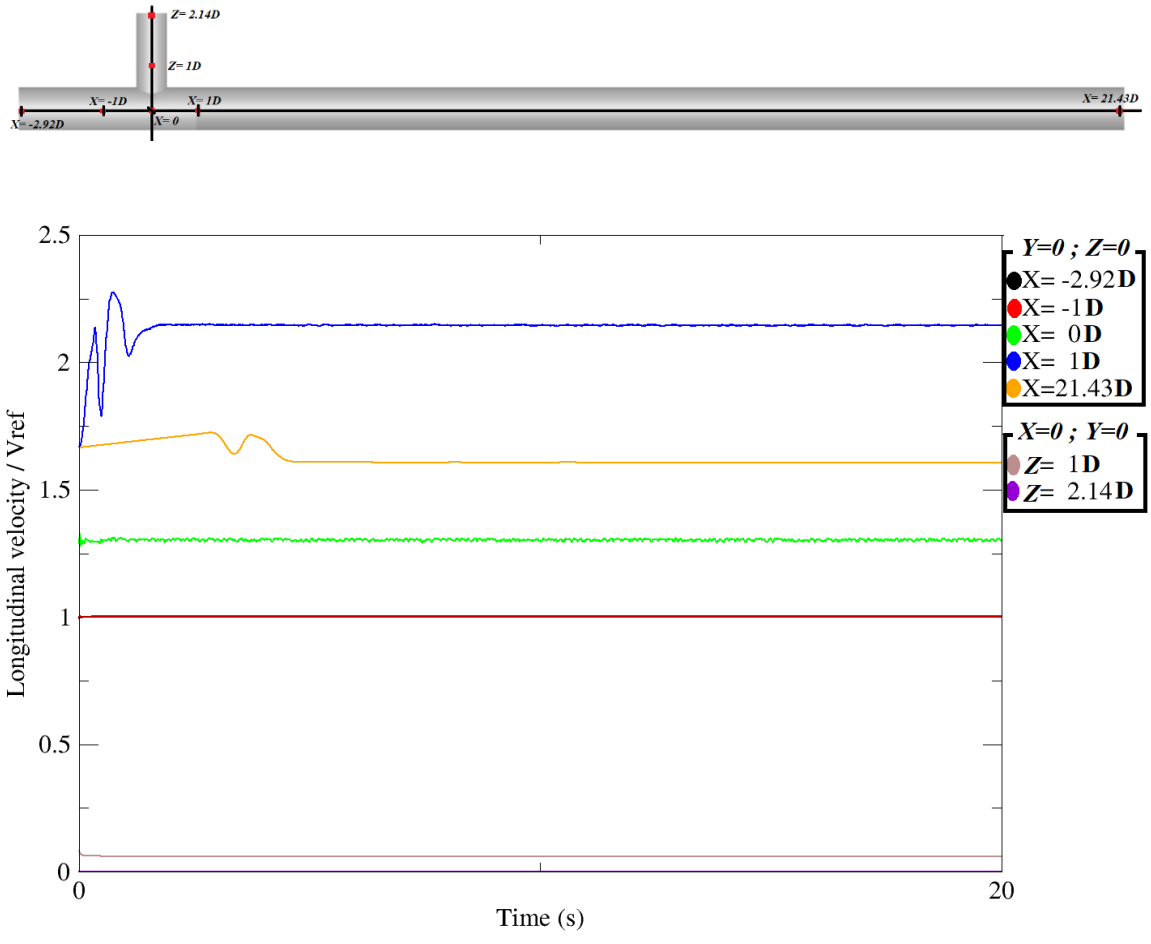

Fig *16*- Longitudinal velocity by time at monitoring points (X and Z axis) for fine mesh

In figure 16 we note that the velocity convergence of the mesh does not affect the convergence of the speed to a fixed value with the passage of time, as most of the large fluctuations in the speed values occurred in the first 10 seconds at most.

And this time period was determined mainly by the farthest monitoring point from the center of the T-junction (brown velocity curve), i.e., at x= 21.50D.

All speed curves converge to an approximately equal value between the fine mesh and the medium mesh, and the difference between them is slight except that the speed comparison at the farthest observation point x = 21.50D m seems different, as it converges to 1.37 in the medium mesh while converging to 1.53 in the fine mesh. This indicates that the distance of the monitoring points from the location of the initial conditions of the calculation gives different results by changing the sensitivity of the mesh, and these differences are noticeable as in our part.

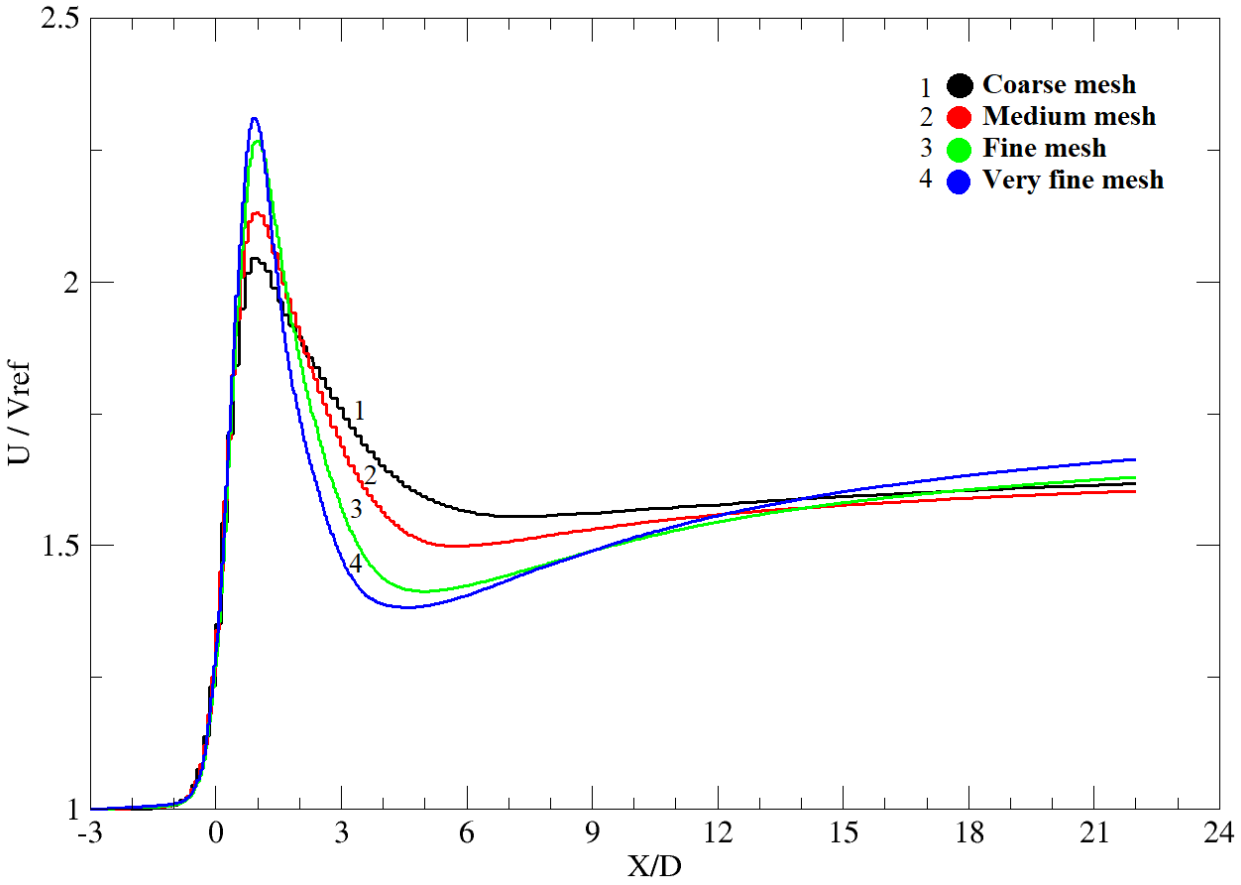

Fig *17*- Longitudinal velocity by x axis for coarse, medium, fine and very fine mesh.

We note that the shape of the X velocity curve has the same shape between the fine mesh and the very fine mesh with a slight deviation, with a consistency in the location of the maximum recorded speed approximately at X=0.50D (Fig 17)

We also note that there is a decrease in the velocity to the lowest value after the T-junction, approximately at X=4.64D, after that the velocity converges to a constant value.

The reason for the velocity increase in this field is that the location of this field is in the vertical tube field (-0.36D < X < 0.36D), as the momentum of the vertical flow is combined with the horizontal flow and the velocity of the vertical and horizontal flows is converted to a horizontal velocity on the x axis, which leads to a gradual and rapid increase in velocity, and near the vertical tube (about X= 0.50D from the center of the T-junction) the velocity reaches a maximum value where the velocities are arranged on the horizontal axis at the center of the tube.

So, starting from here, the observations and analyzes will be based on the results provided by the fine mesh, as these results are more accurate and better than the medium and coarse mesh.

5.1.2 Pressure:

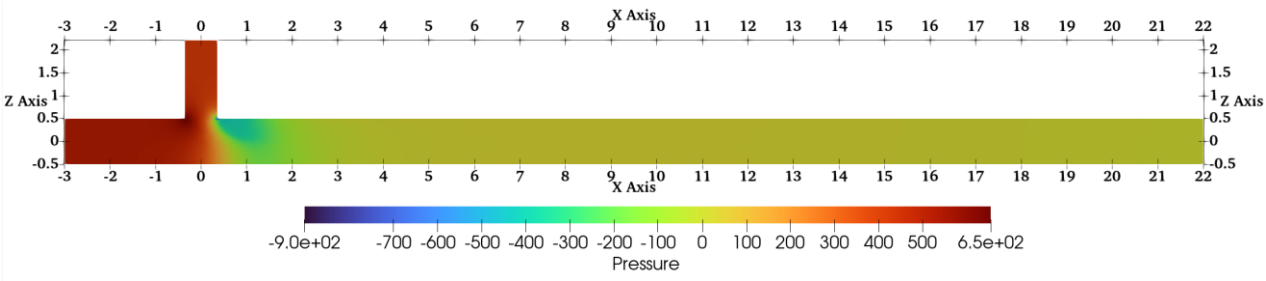

Fig *18*- Pressure field in a XZ plan

The dynamic calculations of this model are logical and this is evident from the figure (Fig 18), where we note that the pressure gradient corresponds to the course of the two flows with the intensification of this gradient in the region after the T-junction (along 1.50D), and we also note that the pressure gradient is not homogeneous with respect to the Z axis, which indicates the presence of eddies in this region, this is due to the presence of the lowest pressure calculated in the upper part of this region (the green color corresponding to the value -400 Pa) and a relatively higher pressure after this region (the orange color corresponding to the value 0 Pa), which makes the flow opposite the direction of the x axis in the upper part, knowing that The flow in the lower part of this region corresponds to the direction of the x axis and thus these two opposite flows in the direction form a vortex in this region.

5.1.3 Velocity magnitude:

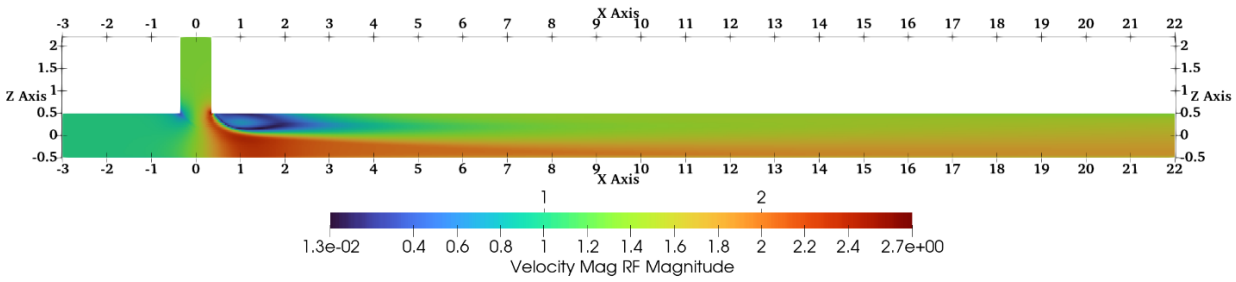

Fig *19*- Velocity magnitude field in a XZ plan

As the velocity magnitude field figure shows (Fig 19), where the eddy is located corresponds to the field in which the pressure gradient is large and it extends to 2D from the center of the T-junction with the calculation of the maximum velocity in the region located between the bottom of the eddy and the bottom wall of the horizontal tube.

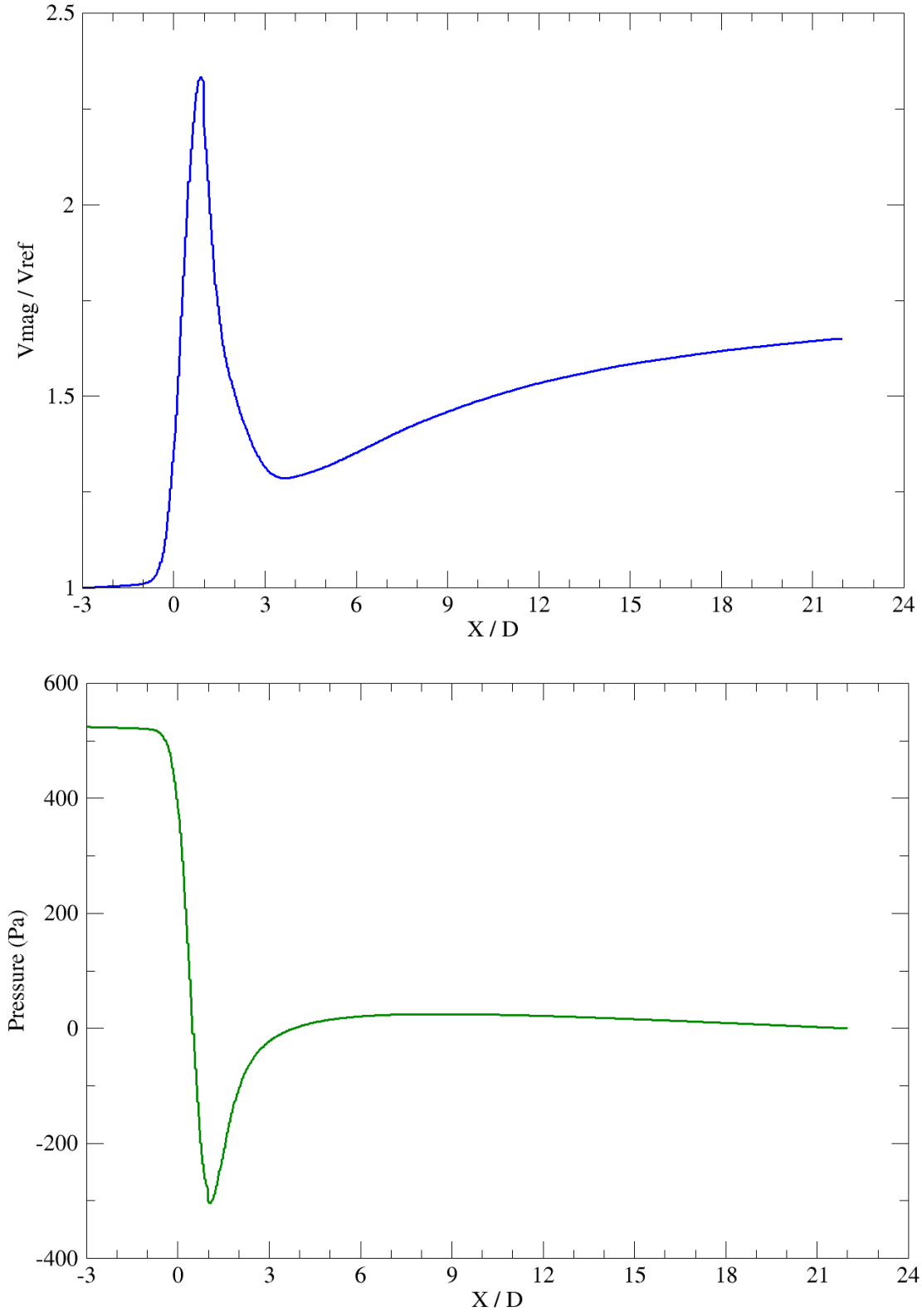

Fig *20*- Variations of the pressure and velocity magnitude by X axis

When we observe the velocity magnitude and pressure curve in (Fig 20), we find that the change of velocity and pressure are opposite in terms of the position on the X-axis, and this reminds us of Bernoulli's law for liquids at a constant temperature ($P + \rho\frac{V^2}{2} = constant$), and this indicates the logical and almost identical results (regardless of fluctuations and energy losses) for theoretical calculations.

-5D < X < -3D The velocity increases slowly in this area due to the suction at the T-junction, while it corresponds to a slow decrease in pressure.

-0.71D < X < 0.36D A rapid increase in velocity with a rapid decrease in pressure due to the presence of the T junction in this area where the summation of two perpendicular flows occurs and the conversion of the velocity components to a horizontal velocity led to a sudden increase in velocity and a significant decrease in pressure

0.36D < X < 0.92D The flow is confined between the first half of eddy and the lower wall of the horizontal tube as it appears as a flow in a tube of decreasing diameter where the velocity increases with decreasing diameter to the maximum value and in this position the diameter of the eddy is perpendicular where it narrows to the two flows coming from the T-junction.

0.92D < X < 3.57D Here the flow is between the second half of the eddy and the lower wall of the horizontal tube, where it plays the role of an increasing diameter tube where the speed decreases and the pressure increase with increasing diameter until the flow reaches the position where the eddy disappears.

3.57D < X < 22D This field is after the eddy, where the diameter of the horizontal tube is fixed and the velocity and pressure converge to a constant value, which is the average of velocity and pressure respectively.

5.1.4 Turbulent viscosity and kinetic energy:

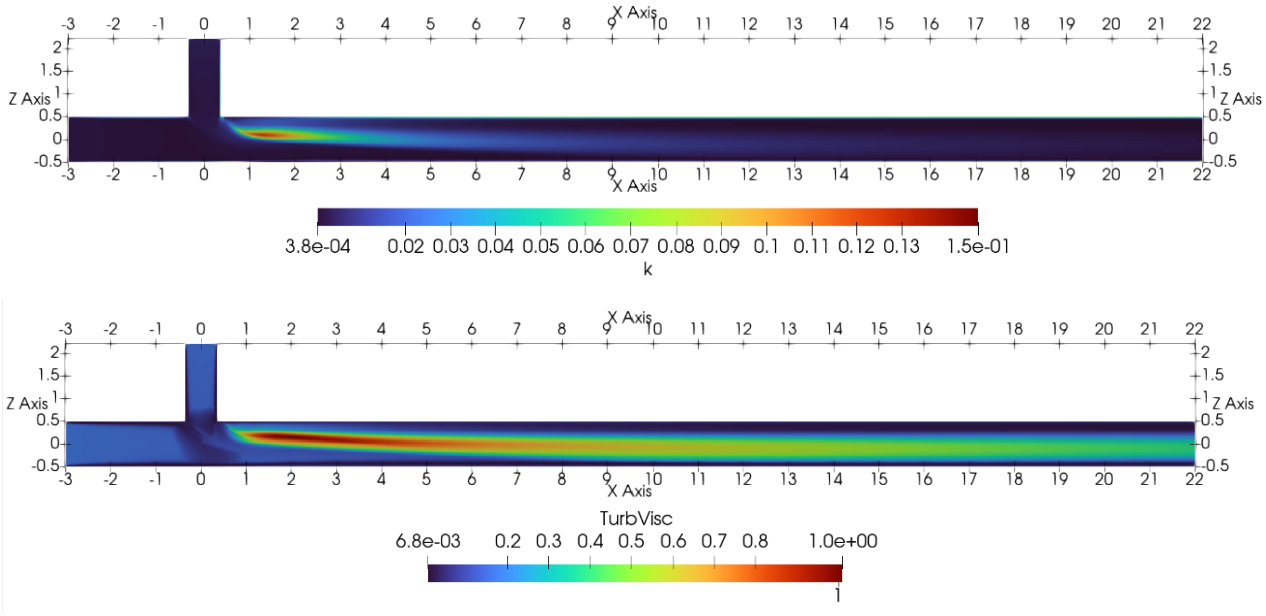

Fig *21*- Kinetic energy and turbulent viscosity field in a XZ plan.

By observing the two figures, we find that the changes of turbulent viscosity and kinetic energy start from the beginning of the T-junction, as we find that they are concentrated in the center of the tube away from the walls, and they take their maximum values at the location of the eddy and its surroundings, while at the two inlets to the beginning of the T-junction we find a flow characterized by small values For turbulent kinetic energy and turbulent viscosity, the T-junction is responsible for mixing events and significant changes in turbulent kinetic energy and the formation of vortices.

When the K-ω-SST model calculates away from the walls, it bases its calculations on the k-ε model and ε is the rate of kinetic energy dissipation and is equivalent to ω where psi can be replaced by ω because w is the specific kinetic energy dissipation rate according to the relationship (ω = ε \ k), and from the figure we notice that the large values of ω are located at the layer adjacent to the walls because the walls suppress the formation of vortices.

5.2 Second part: Thermal and dynamic simulation:

5.2.1 Comparison with experimental results:

Transversal velocity:

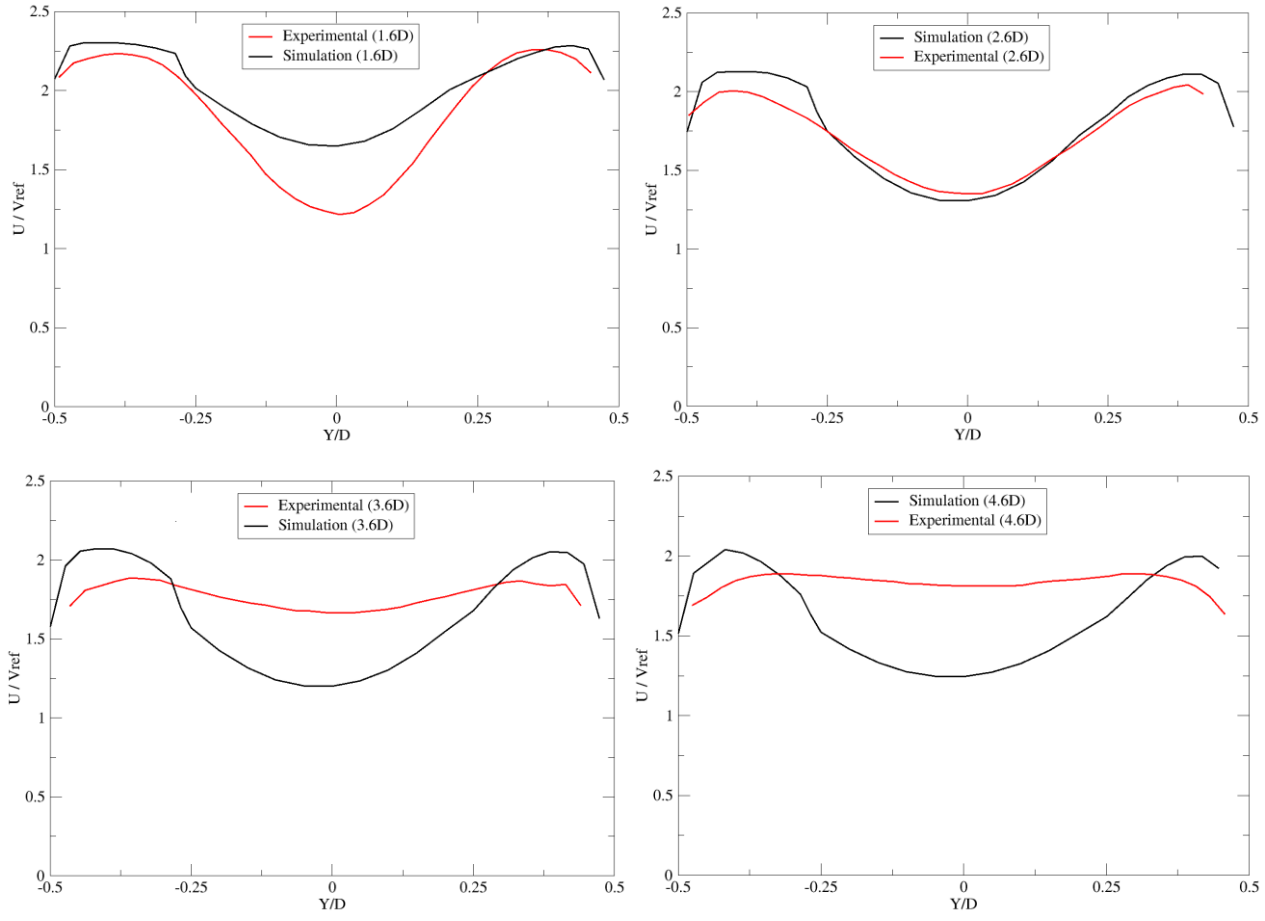

Fig 22**- Comparison of the present study to the experimental results longitudinal velocity by Y axes.**

It is also noted that the results are almost similar to the experimental results, especially at the segment x = 1.60D and x = 2.60D, and this is because these results are as close as possible to the initial conditions and the error begins to appear as we move away from the T-junction, as any small change or approximation in calculation near the initial state will increase with distance from the initial state spatially and temporally.

As for the part near the walls, we note that the velocity gradient in the experimental results is faster than the velocity gradient in the simulation, and this means that the simulator shows a band larger than the experimental results bar, and this is because the velocity is equal to zero at the layer in contact with the walls, whether in the simulation or in the experiment.

Vertical velocity:

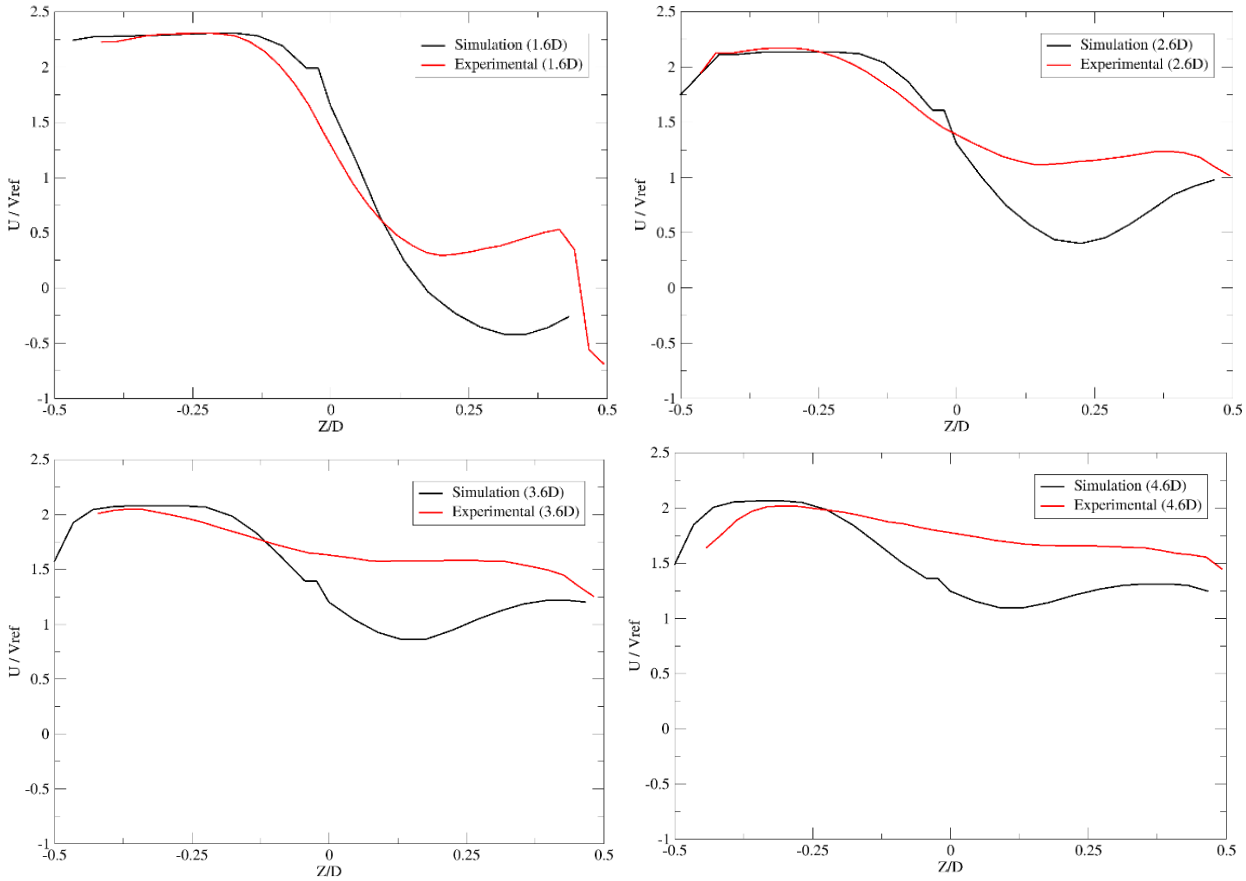

Fig *23*- Comparison of the present study to the experimental results longitudinal velocity by Z axes.

In the above figure, we notice that the simulation shows accurate results in the lower part of the horizontal tube and inaccurate results in the upper part except for the area in contact with the walls because the flow from the vortex that is located at the top of the tube contains large oscillations and large kinetic energy of the turbulence that led to a deviation in the simulation results compared to the experimental results, while the flow in the lower part has a weak kinetic energy of the turbulence, which led to an accurate prediction of the vertical velocity.

Most of the results that are close to the experimental results are found at the center of the tube or near the walls, and this is what the model used mainly focuses on, while we find deviations from the experimental results in other places.

5.2.2 Velocity and pressure:

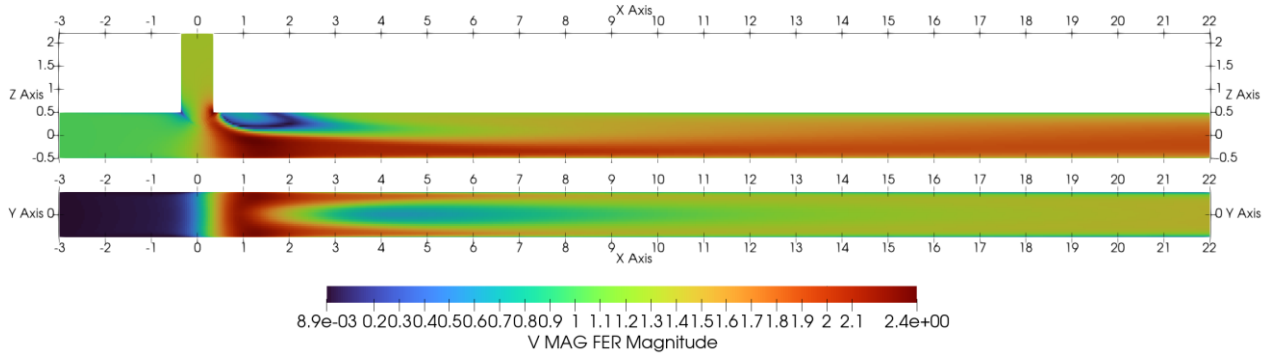

Fig *24*- Velocity magnitude field in a XZ plan and XY plan (From upper to down)

The velocity results appear similar to the velocity results in the dynamics part with slight differences, as the eddy in the dynamic and thermal simulation appears to have a smaller size than the eddy in the dynamic simulation, and the reason for this similarity is due to the relatively small difference in temperature in the two fields as well as the temperature in the dynamic simulation Very close to the average temperature in a dynamic and thermal simulation.

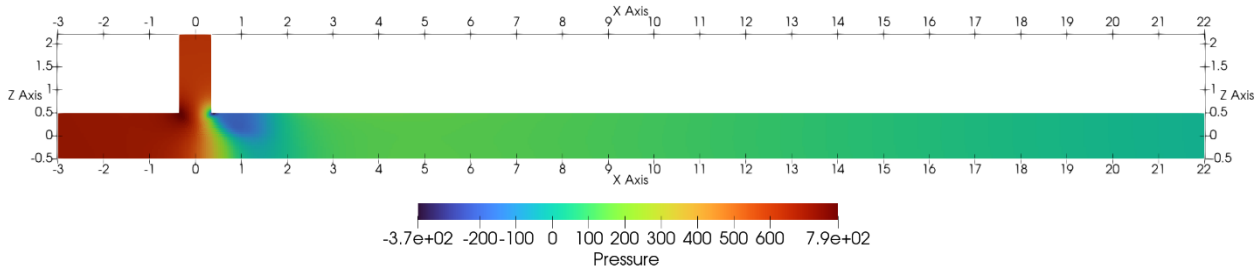

Fig *25*- Pressure field in a XZ plan

By comparing the pressure in the two simulations (Fig 18) and (Fig 23), we note that they have the same spatial distribution shape, but the pressure distribution in the dynamic simulation has a wider range of change than the corresponding in the dynamic and thermal simulation.

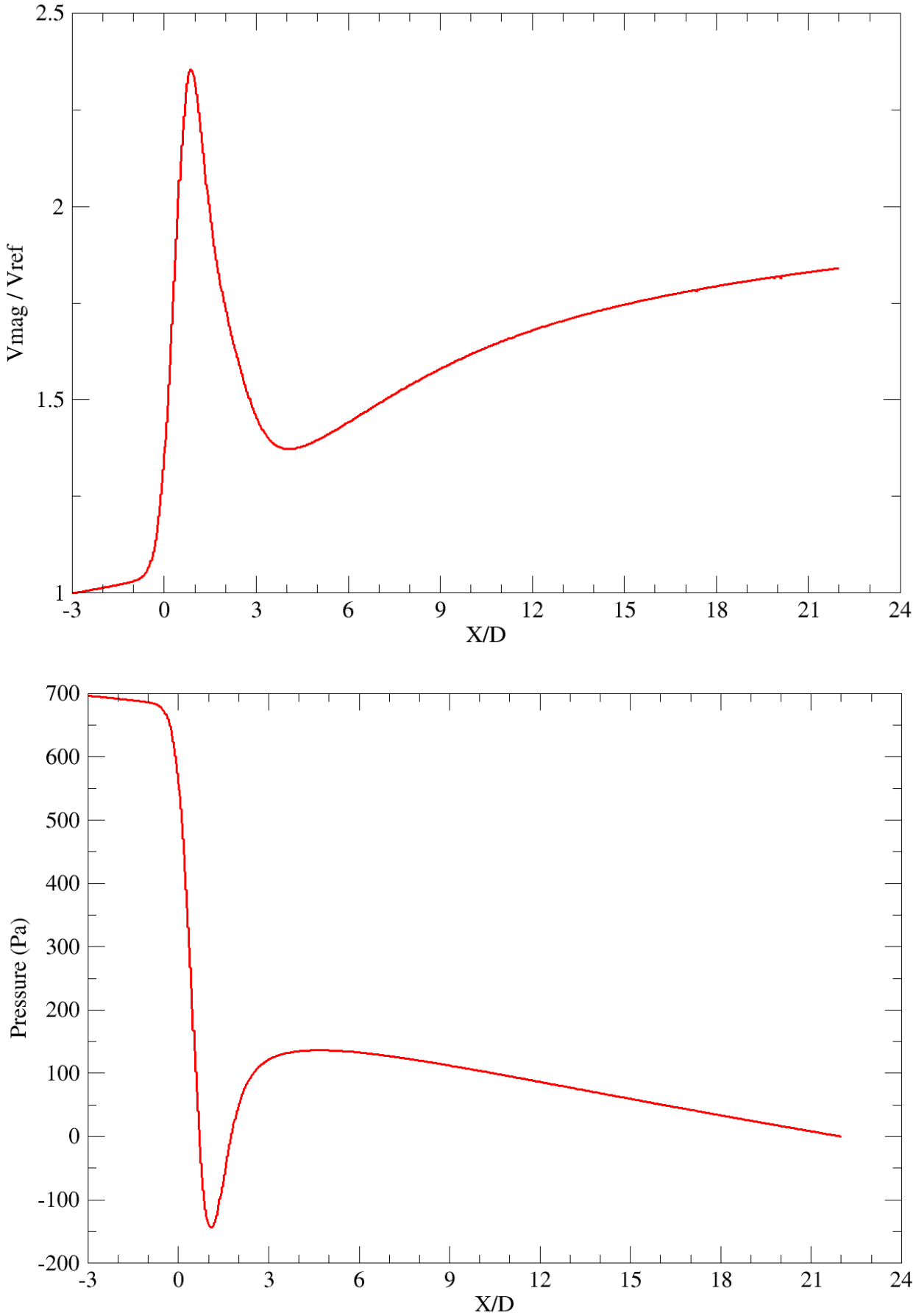

Fig *26*- Pressure and velocity magnitude in terms of the x axis (From upper to down)

Speed changes with a change in the X-axis in the center of the tube seem identical in both simulations (Fig 20) and (Fig 24), because the small difference in temperature and the convergence of the average temperature in both cases does not significantly affect the speed results.

The pressure varies between the two simulations where the pressure at the first inlet in the dynamic and thermal simulation (P_{in1}=700 Pa) is greater than the pressure at the first input in the dynamic simulation (P_{in1}=525 Pa)

Since the first two inputs in the two simulations have the same velocity and temperature difference between them, the density of the liquid is directly responsible for the pressure difference between the two simulations.

Also note that the difference between the minimum value and the maximum value of the pressure after the T-junction is almost the same in the two simulations,

In dynamic and thermal part: P_{max}= 138 Pa and P_{min}= -140 Pa

so $P_{max}-P_{min}=138 - (-140) = 278$ Pa

and in the dynamic part: P_{max}= 25 Pa and P_{min}= -305 Pa

so $P_{max}-P_{min}=25 - (-305) = 330$ Pa

5.2.3 Thermal study:

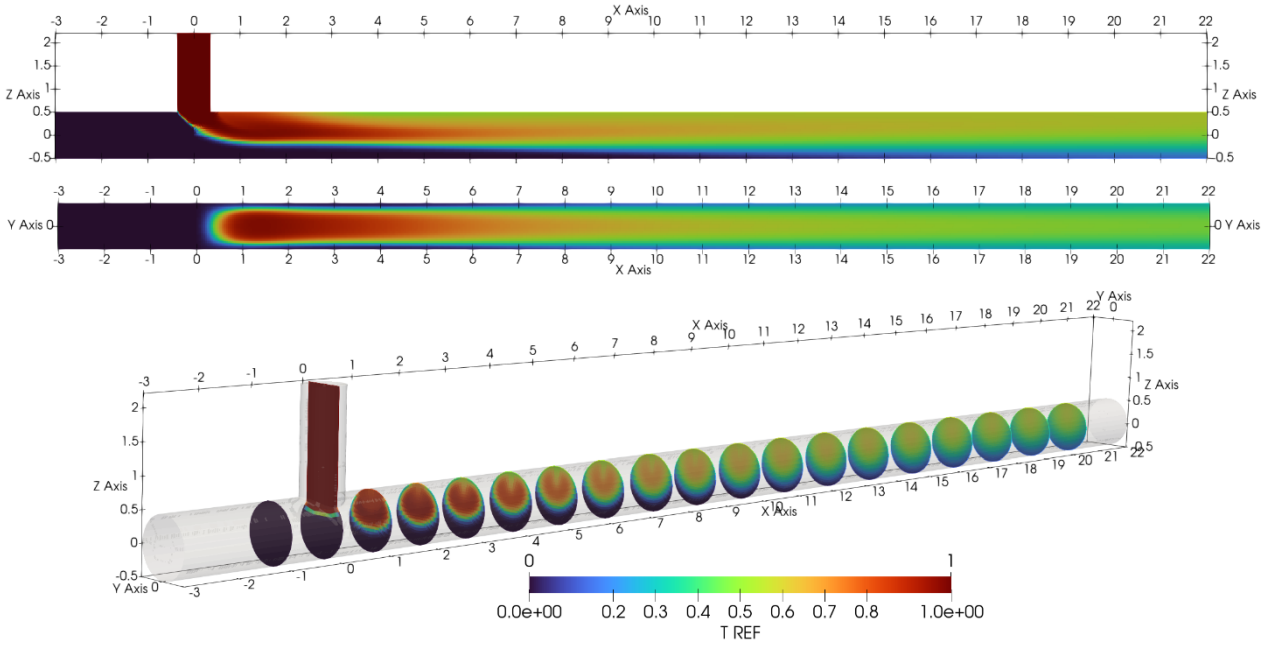

Fig *27*- Temperature field in a XZ plan, XY plan and YZ plan in deferent X positions.

In the above figure, we note that the lower part of the horizontal tube does not contain large thermal fluctuations from its beginning to its end, so we consider that this part is safe from thermal failure and is not responsible for cracks and dents.

Also, in the XY section, we notice the presence of a narrow strip adjacent to the walls that does not contain thermal fluctuations and provides protection for the walls from thermal failure.

While we find that the area's most susceptible to thermal failure are the meeting point of the two inlets in the T-junction at the head of the right angle and It is the part that is often subjected to thermal failure due to the large difference in temperature (T_{min} =19C° and T_{max}=36C°) where it reaches its maximum and because it contains large vibrations due to mixing two speeds orthogonal in the direction and the upper part after the T-junction along the 6D from the end of the T-junction and along this distance there is a large heat exchange between the liquid and the walls of the tube.

The figure of the circular sections (YZ plane) shows us that there is a temperature gradient and that the temperature mixing is not complete, as we find that the cold liquid flows under the hot liquid with a temperature difference of up to 0.3 (30%, 5 degrees Celsius, from 22 to 27 degrees Celsius).

And the last three circular sections show us that there are no significant developments in temperature mixing compared to the previous ones, and if there is a perfect mixing, it will be in a very far range from the T-junction due to the small difference of temperature and the symmetric direction of the two flows.

GENERAL CONCLUSION

General conclusion

In this work, we have used the numerical simulation provided by the free software Code_Saturne to study the flow behavior in the T-junction. The objective of this work is to determine the areas most susceptible to thermal failure, the temperature and pressure distribution, and to determine the mixing locations.

A turbulent flow in a T-junction is numerically carried out using a k-ω-SST turbulence model. The simulation includes two parts; a dynamic and thermal study. The geometry and the boundary conditions are the same for tow simulations. In order to be able to compare our results with experimental studies, we used Vattenfall Research and Development data. A mesh sensitivity test with a comparison of four grids (coarse, medium, fine and very fine) was carried out, to define the best grid to use for our simulations.

It is clear that there is an effect of thermal fluctuations on the turbulent fluid flow, so one focused in identifying the places that contain the most and largest thermal fluctuations.

Regarding to the dynamic results, most of the turbulent vortex eddies structures occur from the center of the T- junction to X=7D (with D = 0.14 m) before they disperse, and it forms a vortex after the end of the T-junction and is considered as dead volume. The obtained results show that the k-ω-SST turbulence model proved its efficiency, as the results are close to the experimental results, especially near the wall. We also note that the thermal fluctuations extend from the center of the T-junction to X=2D, which led to mitigating the turbulent flow range, the upper part of the tjunction at right angles formed by the junction of the two tubes is the most susceptible to thermal failure and vibration. Hot liquid and cold liquid are not mixed perfectly in the T-junction, only slight temperature differences remain.

BIBLIOGRAPHY

[1] **Gustavsson, H.** (2006). Introduction to Turbulence. Division of Fluid Mechanics. Luleå University of Technology Sweden, 2006.

[2] **Tennekes & Lumley** (1972) Cambridge (April 27, 2018) A First Course in Turbulence . 320 pp.,

[3] http://www.ase.uc.edu/~pdisimil/classnotes/Turbulence%202019/ABR_2018%20TURB_C1B_Charateristics_16Jan2019.pdf

[4] **Afgan, I., Kahil, Y., Benhamadouche, S., and Sagaut, P.** (2011). Large eddy simulation of the flow around single and two side-by-side cylinders at subcritical Reynolds numbers. Physics of Fluids, 23, 075101.

[5] **Kahil, Y., Benhamadouche, S., Berrouk, A.S. and Afgan, I.** (2019). Simulation of subcritical-Reynolds-number flow around four cylinders in square arrangement configuration using LES. European Journal of Mechanics/BFluids, 74, 111–122.

[6] **Westin, J.** (2007). Thermal Mixing in a T-Junction. Model Tests at Vattenfall Research and Development AB 2006. Boundary Conditions and List of Available Data for CFD Validation. Vattenfall Memo U 07-26, 2007.

[7] **Kuczaj, A.K., Komen, E.M.J. and Loginov, M.S.** (2010). Large-Eddy Simulation study of turbulent mixing in a T-junction. Nuclear Engineering and Design. 240, 2116–2122.

[8] **Walker, C., Manera, A., Niceno, B., Simiano, M. and Prasser, H.M.** (2010). Steady-state RANS-simulations of the mixing in a T-junction. Nuclear Engineering and Design, 240(9), 2107-2115.

[9] **Aulery, F., Toutant, A., Monod, R., Brillant, G., and Bataille, F.** (2012). Numerical simulations of sodium mixing in a T-junction. Applied Thermal Engineering, 37, 38–43.

[10] **Hüseyin Ayhan, Cemal Niyazi Sökmen** (May 2013) CFD MODELING OF THERMAL MIXING IN T-JUNCTION: EFFECT OF BRANCH PIPE DIAMETER RATIO, Beytepe, Ankara 06800, Turkey

[11] **Howard, R.J.A.,and Serre, E.** (2015). Large-eddy simulation in a mixing tee junction: High-order turbulent statistics analysis. International Journal of Heat and Fluid Flow, 51, 65–77.

[12] **Bessaid, B.S., Dellil, A.Z., Nemdili, F. and Azzi, A.** (2017). Numerical Simulation of Turbulent Thermal Mixing in a Rectangular T-Junction. Computational Thermal Sciences, 9(2), 121–133**.**

[13] **Bello, S.** (2017). Analysis of Fluid-Solid Interaction Contributing to Thermal Fatigue in T-Junction Pipes of Nuclear Power Reactors using STAR-CCM+. Thesis, Department of Nuclear Engineering, University of Ghana. July 2017.

[14] **Cândido, S., and Páscoa, J.** (2020). 3D Unsteady RANS Computation of the Mixing on a T-junction. KnE Engineering, 5(6), 539–546.

[15] **Luaibi, M.S. and Abdulwahid, M.A.** (2021). Numerical Analysis by Computational Fluid Dynamic Simulation of Fluid Flow in A T- Junction. Proceedings of 2nd International Multi-Disciplinary Conference Theme: Integrated Sciences and Technologies, IMDC-IST 2021, 7-9 September 2021, Sakarya, Turkey.

[16] ***Evrim, C., and Laurien, E.*** *(2021). Numerical study of thermal mixing mechanisms in T-junctions. Applied Thermal Engineering, 183, 116155.*

[17] **Marwa S. Luaibi1, Mohammed A. Abdulwahid** (2022) Numerical Analysis by Computational Fluid Dynamic Simulation of Fluid Flow in A T- Junction. Sakarya, Turkey. DOI 10.4108/eai.7-9-2021.2314888

[18] **Menter F. R.**(2011).Turbulence Modeling for Engineering Flows.ANSYS Inc. (Technical Paper 25).

[19] **Gustavsson H.** (2006). Introduction to Turbulence.Division of FluidMechanics, Luleå University of Technology, (Report).

[20] https://www.boldmethod.com/learn-to-fly/aerodynamics/how-to-avoid-wake-turbulence/**:05/09/2022**

[21] **Versteeg H. K.and Malalasekera W.**(2007). An Introduction to Computational Fluid Dynamics: The finite volume method. 2nd Ed. Pearson Education Limited, England

[22] **Fusté R. P.** (2018). Thermal-hydraulic analysis of the ITER Electron Cyclotron Upper Launcher Antenna. Master thesis. Escola Tècnica Superior d'Enginyeria Industrial de Barcelona.

[23] https://www.femto.eu/stories/what-is-cfd/

[24] https://blog.spatial.com/cfd-modeling-applications

[25] https://www.ferrari.com/en-EN/competizioni-gt/articles/tech-insight-cfd-design-in-the-488-gte/:**05/09/2022**

[26] https://redmetal.co.za/engineering-services/computational-fluid-dynamics-flow-simulation/

[27] https://deust.wordpress.com/2011/05/08/introduction-to-computational-fluid-dynamics-cfd/

[28] **Zuo W.** Introduction of Computational Fluid Dynamics. FAU Erlangen-Nürnberg JASS 05, St. Petersburg.

[29] https://www.idealsimulations.com/resources/turbulence-models-in-cfd/

[30] **Jurij S.** (March 2007). Turbulence models in CFD, University of Ljubljana

[31] **Nicoud F.** (2007). Unsteady flows modeling and computation. University Montpellier II and I3M-CNRS UMR 5149, France

[32] https://www.idealsimulations.com/resources/turbulence-models-in-cfd/

[33] **Friess C.** (2010).Modélisation hybride RANS / LES temporelle des écoulements turbulents. Thèse, Université de Poitiers.

[34] **Bouhelal A., Smaïli A.,** (2022). Introduction à la CFD (Computational Fluid Dynamics), National Polytechnic School of Algiers

[35] https://www.cradle-cfd.com/media/column/a168

[36] **Sengupta K., Mashayek F. and Jacobs G.** (2008). Direct Numerical Simulation of Turbulent Flows Using Spectral Method

[37] https://www.cambridge.org/core/journals/journal-of-fluid-mechanics/article/abs/effect-of-phase-change-on-jet-atomization-a-direct-numerical-simulation-study/80ACE4D639B69CF7A3CCD310FB56502D

[38] **Wilcox D. C.** (2006).Turbulence Modeling for CFD, 3rd edition, DCW Industries, Inc, California, USA

[39] https://www.code-saturne.org/cms/

[40] https://www.paraview.org

[41] https://docs.paraview.org/en/latest/UsersGuide

[42] https://plasma-gate.weizmann.ac.il/Grace/doc/UsersGuide

[43] Incropera and DeWitt, Heat and Mass transfer, Fourth edition, 2000.

Abstract:

A turbulent flow in a T-junction is numerically studied using an open source code named Code_Saturne. The study is carried out based on an existing experiment in terms of geometric parameters, fluid properties and initial conditions.

A k-ω-SST turbulence model is used for the simulation and it includes two parts; a dynamic and a thermal study. It is clear that there is an effect of thermal fluctuations on the turbulent fluid flow, so one focused in identifying the places that contain the most and largest thermal fluctuations.

Key words: T-junction, Turbulence, Simulation, Vortex

ملخص:

يتم دراسة التدفق المضطرب عدديًا في تقاطع T باستخدام كود مفتوح المصدر يسمى Code_Saturne. أجريت الدراسة بناءً على تجربة قائمة من حيث المعلمات الهندسية وخصائص السوائل والظروف الأولية.

يستخدم نموذج الاضطراب k-ω-SST في المحاكاة ويتضمن جزأين ؛ دراسة ديناميكية وحرارية. من الواضح أن هناك تأثير للتقلبات الحرارية على تدفق السوائل المضطرب ، لذلك كان التركيز على تحديد الأماكن التي تحتوي على أكبر التقلبات الحرارية.

الكلمات المفتاحية: تقاطع تي , الاضطراب , المحاكاة , الدوامات

Résumé

Une étude d’un écoulement turbulent dans une jonction en T est étudiée numériquement à l'aide d'un code open source nommé Code_Saturne. L'étude est réalisée à partir d'une expérience existante en termes de paramètres géométriques, de propriétés des fluides et de conditions initiales.

Un modèle de turbulence k-ω-SST est utilisé pour la simulation et comprend deux parties ; une étude dynamique et une étude thermique. Il est clair qu'il y a un effet des fluctuations thermiques sur l'écoulement turbulent du fluide, donc on s'est concentré sur l'identification des endroits qui contiennent les plus grandes fluctuations thermiques.

Mots clés: T de mélange, Turbulence, Simulation, Tourbillons